HHS Public Access

Author manuscript

Cancer Cell. Author manuscript; available in PMC 2024 July 11.

Published in final edited form as:

Cancer Cell. 2024 January 08; 42(1): 85–100.e6. doi:10.1016/j.ccell.2023.12.006.

Gut epithelial Interleukin-17 receptor A signaling can modulate distant tumors growth through microbial regulation

Vidhi Chandra[1], **Le Li**[1], **Olivereen Le Roux**[1], **Yu Zhang**[1], **Rian M. Howell**[1], **Dhwani N. Rupani**[1], **Seyda Baydogan**[1], **Haiyan D. Miller**[2], **Erick Riquelme**[1,3], **Joseph Petrosino**[4], **Michael P. Kim**[5], **Krishnan P.L. Bhat**[6], **James R. White**[7], **Jay K. Kolls**[2], **Yuliya Pylayeva-Gupta**[8], **Florencia McAllister**[1,9,10,11]

[1]Department of Clinical Cancer Prevention, University of Texas MD Anderson Cancer Center, Houston TX, USA

[2]Department of Pediatrics and Department of Medicine, Tulane University School of Medicine, New Orleans LA, USA

[3]Department of Respiratory Diseases, Faculty of Medicine, Pontifical Catholic University of Chile, Santiago, Chile

[4]Alkek Center for Metagenomics and Microbiome Research, Department of Molecular Virology and Microbiology, Baylor College of Medicine, Houston TX, USA

[5]Department of Surgical Oncology, University of Texas MD Anderson Cancer Center, Houston TX, USA

[6]Department of Translational Molecular Pathology, University of Texas MD Anderson Cancer Center, Houston TX, USA

[7]Resphera Biosciences, Baltimore MD, USA

[8]Lineberger Comprehensive Cancer Center, The University of North Carolina at Chapel Hill, School of Medicine, Chapel Hill, NC, USA

[9]Department of Gastrointestinal Medical Oncology, University of Texas MD Anderson Cancer Center, Houston TX, USA

[10]Department of Immunology, University of Texas MD Anderson Cancer Center, Houston TX, USA

[11]Lead Contact

SUMMARY

[*]Corresponding author: Florencia McAllister, Department of Clinical Cancer Prevention, University of Texas MD Anderson Cancer Center, 6767 Bertner Ave, Houston, TX 77030, USA, fmcallister@mdanderson.org.

Author contributions

Conceptualization: V.C. and F.M.; Methodology: V.C. and F.M.; Investigation: V.C., L.L., O.L., Y.Z., R.M.H., D.N.R., S.B., H.M., E.R., J.P., M.P.K., K.P.L.B., J.R.W. and J.K.K.; Writing- Original Draft: V.C. and F.M.; Writing- Review & Editing: V.C., L.L., J.K.K., Y.P. and F.M.; Supervision: F.M.; Funding Acquisition: F.M.

Declaration of interests

F.M. is a scientific advisory board member at Neologics Bio. J.R.W. is founder and owner of Resphera Biosciences LLC.

Microbes influence cancer initiation, progression and therapy responsiveness. IL-17 signaling contributes to gut barrier immunity by regulating microbes but also drives tumor growth. A knowledge gap remains regarding the influence of enteric IL-17-IL-17RA signaling and their microbial regulation on the behavior of distant tumors. We demonstrate that gut dysbiosis induced by systemic or gut epithelial deletion of IL-17RA induces growth of pancreatic and brain tumors due to excessive development of Th17, primary source of IL-17 in human and mouse pancreatic ductal adenocarcinoma, as well as B cells that circulate to distant tumors. Microbial dependent IL-17 signaling increases DUOX2 signaling in tumor cells. Inefficacy of pharmacological inhibition of IL-17RA is overcome with targeted microbial ablation that blocks the compensatory loop. These findings demonstrate the complexities of IL-17-IL-17RA signaling in different compartments and the relevance for accounting for its homeostatic host defense function during cancer therapy.

Graphical Abstract

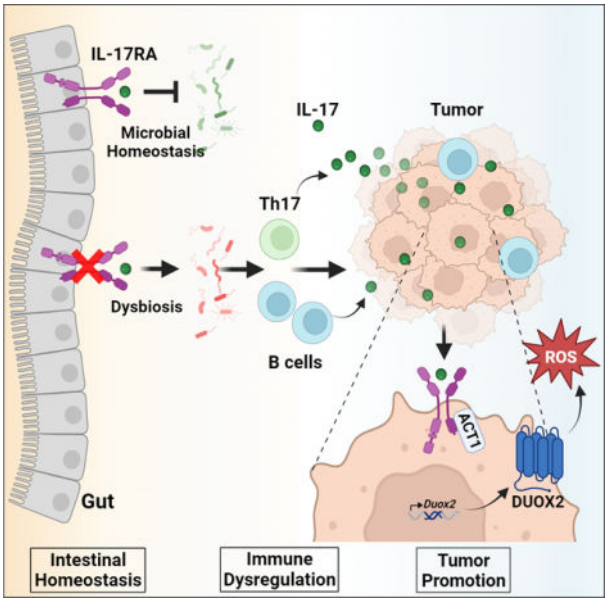

INTRODUCTION

The complex microbial community within the gut interacts with the host facilitating immunity, metabolism, and social behavior to influence human health.[1,2] The gut epithelial barrier is integral for maintaining mucosal immunity, serving as a physical barrier from luminal antigens. Resident immune and epithelial cells secrete immunoglobulins, antimicrobial proteins, and cytokines to regulate intestinal microbes.[2] The production of Interleukin-17 (IL-17) family of proinflammatory cytokines can be triggered by commensal microbes, both bacteria and fungi, under normal physiological conditions and is important for maintaining intestinal homeostasis through regulation of mucosal immunity and gut barrier integrity.[3–5]

IL-17A (or IL-17) and IL-17F homo or heterodimers signal through a complex formed by IL-17 receptor A (IL-17RA) and IL-17RC.[6–8] IL-17RA can also form a complex with IL-17RB to signal through IL-25.[9] IL-17 is mainly secreted by immune cells,[10–16] however, intestinal epithelial and Paneth cells can also secrete IL-17 in response to injury and inflammation to regulate local microbial communities.[17–19] IL-17RA is a multimeric transmembrane glycoprotein[20] that is ubiquitously expressed.[21]

IL-17 is functionally implicated in the pathogenesis of several autoimmune conditions like psoriasis, rheumatoid arthritis, lupus, inflammatory bowel disease, and multiple sclerosis.[22–26] IL-17-IL-17RA signaling has been linked with pancreatic cancer initiation and progression[27–29], as well as immunosuppression and tumor microenvironment (TME) remodeling in established pancreatic ductal adenocarcinoma (PDAC) tumors.[30,31] IL-17 signaling has also been linked to other malignancies including breast,[32,33] liver,[34] lung,[35,36] colon[37–39], and brain cancer.[40] Pathogenic microbes such as enterotoxigenic *Bacteroides fragilis* (ETBF) trigger IL-17 production from immune cells and its signaling through IL-17RA promotes colon tumorigenesis.[37,38,41] In contrast, some studies have reported Th17 mediated anti-tumor immunity in cancers like melanoma and ovarian cancer.[42–44] At the same time, IL-17 producing cells promote $CD8^+$ T cell exhaustion that sensitizes melanoma tumors to immunotherapy.[45] All of these studies highlight that the role of IL-17 in cancer may be context-dependent and contingent on its homeostatic function.

Despite dramatic reduction in tumor growth induced by genetic interventions targeting IL-17-IL-17RA signaling in tumor cells, pharmacological inhibition of IL-17-IL-17RA does not affect tumor growth on its own.[30,38,46] IL-17-IL-17RA blockade has shown anti-tumoral efficacy only in the presence of checkpoint inhibitors.[30] Moreover, the use of interleukin inhibitors in patients with rheumatological conditions has been associated with an increased risk of cancer[47], which further underscores the need for understanding the complex consequences of systemic inhibition of IL-17-IL-17RA signaling.

The microbiota influences progression of PDAC and other tumors.[48–52] Microbial ablation delays pancreatic tumor initiation and growth in murine models[53–55] and antibiotics usage is linked to improved survival in metastatic PDAC patients.[56–58] However, the molecular mechanisms facilitating microbial regulation of tumor behavior remain unknown. Given the known role of IL-17-IL-17RA in maintaining gut homeostasis,[59,60] we hypothesized that enteric IL-17-IL-17RA signaling and its microbial regulation can affect anti-tumoral immunity and ultimately tumor growth. We have interrogated systemic, gut, and tumoral IL-17-IL-17RA signaling pathways through specific compartmental genetic manipulations. Our data reveals the importance of gut microbial homeostasis, immune mechanisms influencing growth of tumors systemically, and the translational relevance of combinatorial targeting of these mechanisms.

RESULTS

Microbially driven elevation of systemic IL-17 promotes pancreatic tumor growth

Our group and others have shown that IL-17 is involved in initiation of pancreatic premalignant lesions, progression, PDAC metastasis, and therapy resistance in murine

models of pancreatic cancer.[27,28,30,31] To determine the role of extra-tumoral IL-17-IL-17RA signaling in pancreatic tumor growth, we performed orthotopic and subcutaneous implantation of KPC cells (LSL-*Kras*$^{G12D/+}$; LSL-*Trp53*$^{R172H/+}$; *Pdx1*-Cre) in global IL-17RA deficient mice (*Il17ra*$^{-/-}$) vs. control mice (*Il17ra*$^{+/+}$) (Figures 1A, S1A). We found that *Il17ra*$^{-/-}$ mice had unexpected significantly increased tumor growth compared to controls in orthotopic (Figures 1B–D) as well as subcutaneous models of PDAC implanted cells with intact IL-17RA (Figures 1E, F). We then performed transcriptomic profiling by RNA-seq that revealed significant upregulation of IL-17 signaling related target genes and pathways in pancreatic tumors which were downregulated in the ilea of *Il17ra*$^{-/-}$ mice compared to controls (Figures 1G, H). We validated the expression of signature genes that are known targets of IL-17 signaling pathway including *Il1b* and *Lcn2* with qPCR and confirmed their upregulation in tumors and downregulation in ilea of *Il17ra*$^{-/-}$ mice (Figure 1I). We further validated higher protein expression of LCN2 in tumors from *Il17ra*$^{-/-}$ mice with immunohistochemical staining (Figure S1B). Using RNAScope we also detected *in situ* higher *Il17a* mRNA expression in tumors and ilea of *Il17ra*$^{-/-}$ mice vs. controls (Figure 1J).

We performed a wide unbiased assessment to detect aberrantly expressed cytokines in circulation and found that IL-17 as well as IL-17F were drastically elevated in *Il17ra*$^{-/-}$ mice compared to controls (Figure 1K) while IL-17 levels failed to increase in heterozygous *Il17ra*$^{+/-}$ mice (Figures S1C). To determine if this effect was unique to IL-17RA-deficient mice, we measured IL-17 in global IL-17RB-deficient (*Il17rb*$^{-/-}$) mice but did not detect an increase in plasma IL-17 levels (Figure S1D). We finally assessed for tumoral *Il17ra* and *Il17rc* expression and found no differences between levels in tumors implanted in global IL-17RA deficient vs. control mice (Figure S1E), suggesting absence of any receptor compensation. Finally, to test the importance of IL-17RC, we orthotopically implanted KPC cells in *Il17rc*$^{-/-}$ mice and observed no change in tumor size compared to control mice (Figure S1F).

Since IL-17 is involved in microbial regulation, we performed gut microbial profiling of *Il17ra*$^{-/-}$ mice that confirmed differences between *Il17ra*$^{+/+}$ and *Il17ra*$^{-/-}$ mice (Figures S1G–I). We then tested if the increase in systemic IL-17 levels was driven by microbes overgrowing in absence of effective IL-17RA signaling. For this purpose, we treated mice with an oral cocktail of anti-bacterial (ampicillin, vancomycin, neomycin and metronidazole) and anti-fungal (amphotericin B) agents that led to a drastic reduction of plasma IL-17 levels in *Il17ra*$^{-/-}$ mice, while levels remained unchanged in *Il17ra*$^{+/+}$ mice (Figure 1L). We subsequently tested single-agent antibiotics and found that ampicillin mimicked the effect of the antibiotics cocktail (Figures 1L, S1H, I).

Based on these results, we hypothesized that the limited efficacy seen with pharmacological IL-17-IL-17RA inhibition may be due to gut microbial dysbiosis. To test this, we combined treatment of monoclonal antibodies against IL-17RA (αIL-17RA) with ampicillin (Figure 1M) to block the compensatory microbial driven IL-17 loop. Single agent treatment with αIL-17RA drastically increased circulating levels of IL-17, which was dampened by coadministration of ampicillin (Figure 1N), similar to results seen in global knockout *Il17ra*$^{-/-}$ mice. While treatment with αIL-17RA alone did not affect tumor growth (Figures

1O, S1J), as previously reported,[30] combination of αIL-17RA with ampicillin resulted in a synergistic anti-tumoral effect (Figures 1O, S1J).

Overall, we found that extra-tumoral absence or blockade of IL-17RA drives IL-17 secretion in response to microbial cues driving systemic IL-17 and growth of pancreatic tumors.

Enteric IL-17RA genetic deletion promotes microbially driven IL-17 signaling dependent pancreatic tumor growth

We then asked whether the pro-tumorigenic effects seen in *Il17ra*$^{-/-}$ mice were due to intestinal microbial dysregulation of IL-17-IL-17RA signaling. To answer this, we generated *Il17ra*$^{fl/fl}$*;Villin-Cre* mice that lacked IL-17RA specifically in intestinal epithelial cells expressing *Villin-Cre* (Figure S2A). The specific enteric deletion was confirmed by immunohistochemical assessment of IL-17RA in ileum and colon (Figure S2B). We then measured circulating IL-17 levels in the plasma of *Il17ra*$^{fl/fl}$*;Villin-Cre* mice and found a significant increase in plasma IL-17 (Figure 2A), although not as marked as in global *Il17ra*$^{-/-}$ mice. We then implanted orthotopic pancreatic tumors in *Il17ra*$^{+/+}$ and *Il17ra*$^{fl/fl}$*;Villin-Cre* mice and assessed tumor growth, in the presence or absence of ampicillin to test for microbial-dependent upregulation of IL-17 (Figure 2B). Similar to our findings in *Il17ra*$^{-/-}$ mice, tumor growth was substantially increased in *Il17ra*$^{fl/fl}$*;Villin-Cre* mice compared to controls and ampicillin treatment abrogated the increase in tumor growth while decreasing plasma levels of IL-17, showing a microbial-dependent effect (Figures 2C–F). The phenotype was also reproduced in a subcutaneous murine model of pancreatic cancer (Figures S2C–E).

To confirm that IL-17 is directly regulating tumor growth, we deleted IL-17RA from KPC cells via CRISPR-Cas9 (KPC$^{Il17ra-/-}$). *Il17ra*$^{fl/fl}$*;Villin-Cre* mice implanted with KPC$^{Il17ra-/-}$ cells failed to increase tumor growth and superseded the use of ampicillin even though IL-17 levels were much higher than ampicillin untreated mice (Figures 2C–F). No significant differences in doubling time were observed in proliferation between KPC$^{Il17ra+/+}$ cells (10.10 h) and KPC$^{Il17ra-/-}$ cells (9.824 h) *in vitro* (Figure S2F), indicative of cell-extrinsic signals available *in vivo* that contribute to IL-17RA dependent tumor growth. As another layer of evidence to confirm relevance of tumor IL-17RA signaling, we deleted the receptor complex adapter protein for IL-17RA signaling, ACT1 (also known as CIKS), and generated KPC cells with ACT1 deletion via CRISPR-Cas9 (KPC$^{Act1-/-}$) (Figure S2G). Similar to IL-17RA deficiency, ACT1 deletion in tumor cells also led to a striking reduction in tumor growth in both *Il17ra*$^{+/+}$ and *Il17ra*$^{fl/fl}$*;Villin-Cre* mice (Figures 2G–I, S2H). This confirmed that specific enteric epithelial IL-17RA deficiency results in gut microbial changes which drive higher production of IL-17 that ultimately promotes growth through IL-17RA signaling in tumor cells.

Transcriptomic profiling with RNA-seq in *Il17ra*$^{fl/fl}$*;Villin-Cre* mice confirmed downregulation of the IL-17 signaling pathway in the ilea along with its upregulation in tumors, in line with findings in global IL-17RA-deficient mice (Figures 2J, S2I). An overlapping reciprocal effect in both *Il17ra*$^{-/-}$ and *Il17ra*$^{fl/fl}$*;Villin-Cre* mice was also seen in the transcriptomic signature of the tumors and ilea for other pathways such as phagosome formation, LPS-IL-1 mediated RXR function, and LXR/RXR activation, suggesting their

IL-17RA dependency (Figure S2J). We then assessed a signature of known IL-17 target genes and found them to be upregulated in tumors of both *Il17ra*$^{fl/fl}$*;Villin-Cre* and *Il17ra*$^{-/-}$ mice while being downregulated in the ilea compared to baseline control tumors and ilea respectively from *Il17ra*$^{+/+}$ mice (Figure 2K). We validated these results by qPCR for *Il1b* and *Lcn2* and found them to be consistently elevated in the tumors while decreased in ilea of *Il17ra*$^{fl/fl}$*;Villin-Cre* mice compared to *Il17ra*$^{+/+}$ mice (Figure S2K), similar to results in global knock-out vs. control mice. We then asked whether the upregulation of IL-17 target genes at the tumor site may be secondary to upregulation of IL-17 receptors in non-enteric sites in the context of specific intestinal deletion of IL-17RA. While we confirmed reduced expression of *Il17ra* mRNA in the ilea of *Il17ra*$^{fl/fl}$*;Villin-Cre* mice and normal levels of *Il17rc*, no compensatory over-expression of *Il17ra or Il17rc* mRNA was seen in the tumors of *Il17ra*$^{fl/fl}$*;Villin-Cre* mice vs. control *Il17ra*$^{+/+}$ mice (Figure S2L). Since tumors were larger in *Il17ra*$^{fl/fl}$*;Villin-Cre* mice but IL-17 levels were not as high as global *Il17ra*$^{-/-}$ mice, we measured plasma IL-17F and found a drastic increase in *Il17ra*$^{fl/fl}$*;Villin-Cre* mice compared to control IL-17RA proficient mice (*Il17ra*$^{+/+}$) (Figure 2L).

While the gut microbial composition of *Il17ra*$^{fl/fl}$*;Villin-Cre* mice was not as markedly altered as in *Il17ra*$^{-/-}$ mice[59] (Figures 2M, S3A, S1H), specific microbes were increased in *Il17ra*$^{fl/fl}$*;Villin-Cre* mice, including *Prevotella* and *Bacteroides* (Figures S3B, C). Previous studies have reported induction of IL-17 producing cells in the gut in the presence of segmented filamentous bacteria (SFB) that is susceptible to vancomycin treatment.[3] All our animals had similar levels of gut SFB which was reduced with vancomycin administration (Figure S3D). Although vancomycin treatment decreased SFB levels, it failed to reduce circulating IL-17 levels in *Il17ra*$^{fl/fl}$*;Villin-Cre* mice (Figure S3E), suggesting that SFB is not responsible for driving the observed phenotype. We then evaluated our known antibiotic capable of modulating IL-17 levels. Ampicillin treatment drastically changed the gut microbiome of both *Il17ra*$^{-/-}$ and *Il17ra*$^{fl/fl}$*;Villin-Cre* mice, including a decrease in *Prevotella* and *Bacteroides* (Figures S3F–J, S1H), suggesting that these microbes may be driving IL-17 in the model, as previously described in other contexts.[61]

To independently test if the IL-17-dependent induction of tumor growth in *Il17ra*$^{fl/fl}$*;Villin-Cre* mice can be modulated, we created parabiotic pairs of control mice joined to *Il17ra*$^{-/-}$ mice or *Il17ra*$^{fl/fl}$*;Villin-Cre* mice (Figure S4A) which share circulation and are co-housed as a product of the surgery model. After a month of successful parabiotic surgery, we subcutaneously implanted KPC cells on both mice in each pair. We expected that increased IL-17 levels from *Il17ra*$^{fl/fl}$*;Villin-Cre* mice would circulate to control parabiotic mouse and result in tumor growth acceleration. The results showed that tumor growth in control parabiont mice was unaffected but *Il17ra*$^{-/-}$ and *Il17ra*$^{fl/fl}$*;Villin-Cre* mice had a complete reversal of increased tumor growth seen in non-parabiont *Il17ra*$^{fl/fl}$*;Villin-Cre* mice (Figures S4B, C). We then measured plasma IL-17 levels and found a significant reduction in both parabiont *Il17ra*$^{-/-}$ and *Il17ra*$^{fl/fl}$*;Villin-Cre* mice compared to pre-parabiotic time point or control parabiont *Il17ra*$^{+/+}$ (Figures S4D, E). This data confirmed that circulating IL-17 triggered by intestinal microbial changes can regulate tumor growth systemically.

Intestinal IL-17-IL-17RA dependent microbial dysbiosis can affect tumor growth remotely

Our findings revealed that disruption of microbial homeostasis due to deficient enteric IL-17-IL-17RA signaling can affect tumor growth outside the colon, so we tested if tumors in sites remote from the gastrointestinal tract like the brain could also be influenced. Intestinal microbes and IL-17 signaling are well known to be important during neurological conditions such as autoimmune encephalitis.[26,62] Increased levels of IL-17 and infiltrating Th17 cells have also been described in murine and human glioblastoma (GBM).[40,63] We investigated orthotopic tumor growth with syngeneic murine glioma cells- Gl261 in recipient *Il17ra*$^{+/+}$, *Il17ra*$^{-/-}$ and *Il17ra*$^{fl/fl}$*;Villin-Cre* mice (Figure 3A). Similar to our findings with pancreatic tumors, global *Il17ra*$^{-/-}$ deficient mice had significantly faster tumor growth compared to *Il17ra*$^{+/+}$ mice, while *Il17ra*$^{fl/fl}$*;Villin-Cre* mice experienced the most aggressive tumor growth (Figures 3B–E). We also assessed neurological signs/symptoms and found significant reduction in reflexes in *Il17ra*$^{fl/fl}$*;Villin-Cre* mice and spontaneous seizures were observed in 20% of *Il17ra*$^{-/-}$, 50% of *Il17ra*$^{fl/fl}$*;Villin-Cre* mice, which were normal in control mice (Figures 3F–G). IL-17 related genes, previously described in neurological conditions such as *Cd4*, *Duoxa2*, *Igfbp3*, *Mmp9*, *Pde9a* and *Slc35f2* were increased in the tumors, while decreased in matched ilea of both *Il17ra*$^{-/-}$ and *Il17ra*$^{fl/fl}$*;Villin-Cre* mice compared to *Il17ra*$^{+/+}$ mice (Figure 3H). Overall, disruption of homeostatic intestinal IL-17-IL-17RA signaling accelerated growth of brain tumors.

We then searched for ileal transcriptomic changes in pancreatic (PDAC) and brain (GBM) tumor-bearing *Il17ra*$^{fl/fl}$*;Villin-Cre* mice. We found antimicrobial humoral and defense responses as main overlapping pathways downregulated in the ilea of *Il17ra*$^{fl/fl}$*;Villin-Cre* mice bearing PDAC or GBM (Figure S4F). We then assessed the effect imposed by intestinal IL-17-IL-17RA deficiency on IL-17-related genes in different tumor types. We found higher expression of genes such as *Duoxa2* and *Lcn2* in PDAC while *Rbp4* and *Spdef* were elevated in GBM, compared to *Il17ra*$^{+/+}$ mice bearing PDAC or GBM tumors, respectively (Figure S4G). This data illustrates the unique signals that drive tumor growth in different niches and tumor microenvironments in the context of the same upstream microbial and immunological triggers.

Enteric IL-17RA deficiency triggers B cells development

We then proceeded with unbiased immunoprofiling based on CyTOF and flow cytometry to determine how major immune cell populations are rewired in the absence of effective enteric IL-17-IL-17RA signaling which could help explain the tumor-promoting effect. For this purpose, we obtained single cells after digestion of matched ilea and pancreatic orthotopic tumors harvested at an early stage when tumor size was similar between groups (Figure 4A).

While most major immune cell populations were similar between groups, CyTOF showed a significant increase in B cells in the lamina propria (LP) and tumors from *Il17ra*$^{fl/fl}$*;Villin-Cre* mice (Figures 4B–E, Table S1). We confirmed increase in tumor infiltrating B cells by flow cytometry (Figures 4F, G, S5A–C). Mesenteric lymph nodes (mLN) and splenic tissue from enteric IL-17RA-deficient mice also had increased B cells (Figures 4G, S5D–G). We also performed immunohistochemical staining for CD20 in orthotopic pancreatic tumors which revealed higher number of B cells infiltrating *Il17ra*$^{-/-}$ and *Il17ra*$^{fl/fl}$*;Villin-Cre* mice

vs. control mice (Figures 4H, S5H). Abundance of B cells in tumors had a significant positive correlation with tumor volume in *Il17ra*$^{fl/fl}$*;Villin-Cre* mice, suggesting that B cells may play a pro-tumorigenic role in pancreatic tumors (Figures S5I). To determine if B cells generated in the gut could also infiltrate remote tumors, we assessed GBM tumors in *Il17ra*$^{-/-}$ and *Il17ra*$^{fl/fl}$*;Villin-Cre* mice and found significantly higher infiltration of B cells compared to control *Il17ra*$^{+/+}$ mice (Figures S5J, K).

To ultimately test the functional relevance of B cells in influencing tumor growth, we depleted B cells *in vivo* using neutralizing antibodies against CD20 in a PDAC subcutaneous model (Figure 4I). We confirmed reduction of B cells by flow cytometry in all compartments including tumors, LP, mLN, spleen and Peyer's Patches (PP) (Figures 4J, S5L–P). Depletion of B cells stunted the increase in tumor growth seen in *Il17ra*$^{fl/fl}$*;Villin-Cre* mice but augmented tumor growth in control *Il17ra*$^{+/+}$ mice (Figures 4K, S5Q), suggesting that B cells generated in the absence of effective IL-17-IL-17RA intestinal signaling have tumor promoting capacity.

Th17 and B cells are main sources of IL-17A and IL-17F in tumors

Given our data showing increased IL-17 in plasma and transcriptomic changes showing modulation of IL-17 targets in *Il17ra*$^{fl/fl}$*;Villin-Cre* mice that have larger tumors, as well as previous reports showing increase in intestinal IL-17 secreting cells in these animals, we used single cell sequencing (scRNA-seq) to determine if IL-17-expressing cells are infiltrating tumors as well (Figures 5A, S6A, B). We found higher numbers of *Il17a* expressing immune cells in gut and tumors while *Il17f* expressing immune cells were higher only in tumors from *Il17ra*$^{fl/fl}$*;Villin-Cre* mice vs. controls (Figure S6C).

We then aimed to determine the cellular source of IL-17 in our model (Figures 5B, C). Assessment of the lamina propria (gut) showed that expression of both *Il17a* and *Il17f* was restricted to Th17 cells in *Il17ra*$^{fl/fl}$*;Villin-Cre* mice (Figures 5D, S6C), as previously described.[59] We then examined the immune cells infiltrating tumors and found *Il17a* was primarily expressed in CD4^{+} T cells (Th17 cells) while *Il17f* was found in Th17 and B cells (Figures 5D, S6C). We then performed RNA *in situ* hybridization to validate this finding and detected higher number of *Il17a* and *Il17f* expressing cells in tumors from *Il17ra*$^{fl/fl}$*;Villin-Cre* vs. control mice (Figure 5E). Moreover, we confirmed the presence of B cells expressing IL-17F within tumors by co-detection of *Il17f* in CD20^{+} cells (Figure 5F).

Transcriptomic analysis of B cells in the lamina propria from *Il17ra*$^{fl/fl}$*;Villin-Cre* mice revealed decreased adaptive, humoral and microbial defense responses compared to control mice (Figure S5D). Similarly, tumor infiltrating B cells exhibited reduced defense to bacteria, lipopolysaccharide and anti-microbial humoral responses (Figure 5G). Intrinsic B cell signaling has been shown to determine its effector function during PDAC.[64] We examined tumor B cell sub cluster expressing IL-17F which showed decreased anti-microbial humoral response and intrinsic apoptotic signaling, indicating potential cellular dysfunctionality (Figures S6E, F). We examined transcription factors capable of inducing IL-17F production and found higher levels of *Runx1* and *Stat3* but absence of *Rora* and *Rorc* expression (Figures S6G, H). B cells that expressed *Il17f* did not co-express *Il10* (Figure S6G), a marker for B regulatory cells. Thus, data suggests that intestinal microbial dysbiosis

in the setting of ineffective IL-17-IL-17RA signaling triggers gut development of Th17 cells and B cells, main sources of IL-17A and IL-17F, which can circulate systemically and infiltrate tumors.

Enteric IL-17RA deficiency mediated IL-17 secretion increases Duox2 signaling in pancreatic tumors.

We then aimed to dissect transcriptional changes occurring in tumor cells that may mechanistically explain the larger tumors observed in mice with enteric IL-17RA deficiency. We examined differential gene expression in tumor cells cluster 1 in *Il17ra*$^{fl/fl}$*;Villin-Cre* vs. control mice and found downregulation of pathways related to response to interferons and upregulation of responses to growth factor stimulus and interaction with symbiont (Figure S7A). To prioritize IL-17 driven genes/pathways, we compared our single cell gene expression data with previously reported IL-17 driven pancreatic datasets.[27,30] These comparisons revealed *Duox2* as the common gene differentially regulated by IL-17 (Figure 5H) and primarily expressed in tumor cell clusters from *Il17ra*$^{fl/fl}$*;Villin-Cre* mice by single cell analysis (Figures 5I, S7B). Pathway analysis of tumor cells in cluster 1 with high vs. low *Duox2* expression revealed higher catalytic activity, response to DNA damage, hydrolase activity, and Wnt signaling, but decreased response to bacteria (Figure 5J, S7C).

DUOX2 is an oxidase enzyme described to be under the control of IL-17RA signaling.[65] As a validation functional experiment, we used tdTomato fluorescent mice implanted with non-fluorescent orthotopic pancreatic cancer cells and treated them with αIL-17A/αIL-17RA antibodies (Figures 5K). We sorted non-fluorescent tumor cells, to exclude stromal and immune populations (Figures S7D). We confirmed downregulation of both *Duox2* and its maturation factor *Duoxa2* in enriched tumor cells upon IL-17 blockade (Figure 5L). Direct exposure of KPC cells to IL-17 *in vitro* led to an increase in oxidase genes such as *Nox1, Nox2, Noxa1, Duox1, Duox2, Duoxa1*, and *Duoxa2* (Figure S7E). IL-17 treatment also drastically increased ROS (Figures S6F–H) and H_2O_2 production by KPC cells which was lost when the cells lacked the IL-17RA receptor (Figures 5M, S7I).

Human PDAC has circulating and tumor infiltrating cells that express IL17, whose levels associate with DUOX2.

We then investigated the cellular source of IL-17 at single cell level in human PDAC. We performed spatial single cell transcriptomic analysis on primary PDAC using CosMx Spatial Molecular Imaging (SMI) technology to create a comprehensive spatial PDAC IL-17 atlas (Figure 6A). We identified diverse cell types in human PDAC including tumor cells, pancreatic endocrine cells, stromal, and several types of immune cells (Figure 6B). Next, we evaluated sub-cellular gene expression by cell type and found that *IL17A* transcripts were predominantly expressed in T cells while other immune cells such as plasma, myeloid, and mast cells had low expression (Figures 6B, C). We then evaluated IL-17 producing immune cells in circulation in PDAC patients. Flow cytometric analysis of peripheral blood showed that PDAC patients have elevated levels of IL-17 secreting immune cells (IL-17A$^+$ and IL-17A$^+$/IL-17F$^+$) compared to healthy controls (Figures S7J–L).

Finally, we examined the TCGA database and stratified human PDAC according to *IL17A* expression and found significantly higher *DUOX2* expression in tissue with higher *IL17A* expression (Figure 6D). Subsequently, based on average *DUOX2* expression, we classified PDAC according to high vs. low *DUOX2* expression and extracted the differentially expressed genes. Pathway analysis using those genes revealed reduced response to lipopolysaccharide, bacteria, and oxygen containing compounds in high *DUOX2* expressing PDAC (Figures 6E, F). To determine if PDAC-associated gut microbes may also have the potential to drive systemic IL-17 signaling, we compared data from publicly available datasets to gut microbes of PDAC bearing *Il17ra*$^{fl/fl}$*;Villin-Cre* mice.[68,69] We found that taxa such as Bacteroides were enriched in both settings (Figure S7M), implying that gut microbes in PDAC patients are similar to those increased in the context of gut epithelial deletion of IL-17RA and elevated IL-17. It also suggests that gut microbes cleared by IL-17 could potentially contribute to PDAC pathogenesis. Overall, these findings underscore the clinical relevance of IL-17 dependent signal transduction in cancer cells, which can modulate responses to microbes.

DISCUSSION

The microbiota is well recognized for its functional role in the pathogenesis of cancer, host tumor immune responses, and therapy responses.[2,48,66] IL-17 signaling is vital for microbial clearance and maintenance of intestinal barrier immunity and its dysregulation can have deleterious consequences.[5] IL-17-IL-17RA signaling is delicately balanced to achieve precise maintenance of barrier immunity and prevent immune hyperactivity.

Mice with global genetic deletion of IL-17RA, mimicking the effect of systemic IL-17 inhibition, experience gut dysbiosis and elevated IL-17 production due to inefficient gut microbial clearance that ultimately results in increased growth of IL-17RA proficient tumors. Our model of enteric epithelial deletion of IL-17RA served to uncouple its role in intestinal epithelium and revealed an even stronger tumor promoting effect in distant organs like the brain or pancreas. This tumor promoting effect in the pancreas was reversed by deletion of IL-17RA or ACT1 in cancer cells or with targeted microbial depletion. Overall, we demonstrated in two tumor types that aberrant intestinal epithelial IL-17RA signaling leads to systemic dysbiotic immune signaling that can funnel into tumors cells proficient for IL-17RA signaling to augment their growth. The disparity in the tumor burden between *Il17ra*$^{fl/fl}$*;Villin-Cre* and *Il17ra*$^{-/-}$ mice can be attributed to the contribution of IL-17 signaling through non-tumoral cells (immune or stromal) with intact IL-17RA in mice in mice with enteric deficiency.

Patients treated with IL-17 inhibitors have been found to have increased levels of IL-17 in the gut mucosa.[67] Both murine and human data suggests that inhibition of this pathway induces a counteracting IL-17-mediated response that would oppose IL-17 monoclonal antibodies and likely explains the inefficacy observed in the clinic.[46] In our model, pharmacological inhibition of IL-17RA with neutralizing monoclonal antibody did not lead to increased tumor growth, as observed in global knockout mice, since IL-17RA in tumor cells was also inhibited. Long term use of these drugs, capable of altering gut microbial balance and increase in systemic IL17-secreting cells, could result in pro-tumorigenic

effects. Addition of targeted microbial depletion to decrease that counteracting IL-17 loop resulted in reduction of tumor size when given concomitantly with αIL-17RA antibodies.

We found that IL-17 is primarily produced by T cells (Th17) in both murine and human datasets through single cell analysis. Importantly, circulating levels of IL-17F were significantly increased in the *Il17ra*$^{fl/fl}$*;Villin-Cre* mice and higher *Il17f* mRNA expression was detected in their pancreatic tumors. We found that CD4^{+} T cells and B cells were the main sources of IL-17F producing cells (Th17 and B^{17F}) in the tumors. Since deletion of IL-17RA in tumor cells reverses the phenotype, we predict that the tumor growth phenotype may be dependent on both IL-17A and IL-17F in the global *Il17ra*$^{-/-}$ while dependent on IL-17F in the enteric epithelial IL-17RA deficient *Il17ra*$^{fl/fl}$*;Villin-Cre* mice. Genetic deletion of IL-17A in a spontaneous tumorigenesis model of pancreatic malignancy also led to a compensatory increase in systemic levels of IL-17F,[31] which could explain the absence of delayed tumorigenesis in that model.

The expansion of B cells unique to *Il17ra*$^{fl/fl}$*;Villin-Cre* mice may be explained by the increase in IL-17A which can signal through IL-17RA in B cells and stimulate their differentiation in absence of effective enteric IL-17-IL-17RA signaling and the resulting gut dysbiosis. The role of IL-17 in influencing B cell differentiation, affecting their immunoglobulin production and antibody class switching has been previously reported.[70] The tumor promoting role of B cells during pancreatic cancer has also been described.[64,71,72] Our data suggests that, in the absence of effective enteric IL-17 signaling, other cell types with microbial defense functionality, like B cells, can be triggered in the gut and migrate to remote sites including tumors.

DUOX2 is a NADPH dual oxidase involved in ROS generation and pathogen defense.[73] DUOX2 is involved in maintaining mucosal immunity and aids in anti-bacterial responses.[65,74] Patients with intestinal bowel disease (IBD) have increased gut expression of DUOX2.[75] Additionally, intestinal DUOX2 is under the control of IL-17RA signaling.[65] DUOX2 expression in pancreatic tumor cells has been linked to increased tumorigenic potential and associated with worse prognosis.[76–78] IL-17-secreting cells can increase DUOX2 signaling and ROS production through signaling on tumor cells. Importantly, *DUOX2* levels are linked to microbial defense and strongly associated with *IL17A* in human PDAC.

Since 2015, the Food and Drug Administration (FDA) approved the use of monoclonal antibodies against IL-17 in patients with autoimmune disease like plaque psoriasis, ankylosing spondylitis, and psoriatic arthritis. Clinical attempts to block IL-17 signaling during gastrointestinal conditions such as Crohn's disease or spondylarthritis using single-agent clinical monoclonal antibodies targeting IL-17A with secukinumab[79] or IL-17RA with brodalumab[80] have been largely unsuccessful, often accompanied with aggravated inflammatory intestinal symptoms. A meta-analysis examined 74 clinical trials comprising of patients with rheumatological conditions being treated with interleukin inhibitors and found an increased risk of serious and opportunistic infections as well as cancer in treated patients compared to placebo controls.[47]

This manuscript reveals a mechanism of resistance to cytokine inhibition in cancer which may not necessarily be restricted to IL-17 inhibition and may explain failure of several other trials using inhibitors of essential host defense cytokines in cancer. Future trials may combine IL-17 inhibition with antibiotics to reduce burden of microbes not cleared by IL-17 or fecal microbial transplantation from healthy donors with two goals: 1) block the compensatory IL-17 loop which would enhance the efficacy of IL-17 inhibitors, and 2) decrease abundance of microbes present in PDAC patients which are also linked to tumor promotion.[51]

In summary, we demonstrate that intestinal IL-17-IL-17RA signaling is crucial for microbial homeostasis and its inhibition can negate systemic anti-tumoral effects. Future studies targeting IL-17 or even other cytokines may need to take this into consideration.

Limitations of Study

The current study does not explore the role of IL-17RA on immune cells and how it may impact tumor immunity in the context of gut dysbiosis. Additionally, the specific role of circulating IL-17F and IL-17F producing B cells for regulation of microbes and tumor growth is not specifically dissected. It is of note that only implantable cancer models were utilized in this study, and further studies should explore these mechanisms during tumor initiation and progression in models of spontaneous tumorigenesis. Finally, mechanisms utilized by cancer cells for DUOX2 dependent microbial regulation in the TME needs further examination.

STAR METHODS

RESOURCE AVAILABILITY

Lead contact—Further information and requests for resources and reagents should be directed to and will be fulfilled by the lead contact, Florencia McAllister (fmcallister@mdanderson.org).

Materials availability—Mouse cell lines generated in this study are available upon request with a completed Materials Transfer Agreement.

Data and Code availability—The RNA sequencing data are being deposited in the Sequence Read Archive (NCBI SRA under BioProject accession no. PRJNA1039869). This paper does not report original code. Any additional information required to reanalyze the data reported in this paper is available from the lead contact upon request.

EXPERIMENTAL MODEL AND STUDY PARTICIPANT DETAILS

Human Samples—Buffy Coat: Peripheral whole blood samples were collected in EDTA Collection Tubes and centrifuged to collect buffy coat cells from the interphase and stored at −80°C until use. PDAC: Archived Formalin-fixed paraffin embedded (FFPE) primary tumors were used from patients who underwent surgical resection. All protocols were approved by the Institutional Review Board at University of Texas MD Anderson Cancer Center.

Genetically Engineered Mice—All animal experiments were conducted in compliance with the National Institutes of Health guidelines for animal research and were approved by the Institutional Animal Care and Use Committee of The University of Texas MD Anderson Cancer Center. All studies were conducted using mice with C57BL/6 genetic background. WT and *Il17ra*$^{-/-}$ mice were obtained from Taconic Biosciences, deposited by Amgen Inc. *Il17rc*$^{-/-}$ mice were obtained from Charles River Laboratories, deposited by Amgen Inc. mTmG mice were obtained from The Jackson Laboratory. *Il17ra*$^{fl/fl}$ mice were crossed with *Villin-Cre* mice to obtain *Il17ra*$^{fl/fl}$*;Villin-Cre*. Mice of both sexes were used at 10–30 weeks with age and litter matched *Il17ra*$^{+/+}$ controls. All mice of different genotypes and treatments were housed in separate cages post weaning with Enviro-dri bedding (Shepherd Specialty Papers). Genotyping was done according to vendor's instructions (Figures S1A, S2A).

Cell Lines—Murine PDAC KPC (KPC$^{Il17ra+/+}$) (LSL-*Kras*$^{G12D/+}$; LSL-*Trp53*$^{R172H/+}$; *Pdx1*-Cre) cells were cultivated in DMEM media with 4.5 g/L glucose (Corning) supplemented with 10% FBS (Sigma-Aldrich) and no antibiotics at 37°C and 5% CO_2 in a humidified atmosphere. KPC$^{Il17ra-/-}$ were generated with CRISPR-Cas9 technology as described previously.[30] Targeted knockout of ACT1 in KPC cells was performed with mouse *Traf3ip2* CRISPR-Cas9 plasmid (KN318215G1, OriGene Technologies) following manufacturer's instructions. Single cell clones were confirmed by Western blotting with anti-ACT1 antibody (TA323297, OriGene Technologies). Murine glioma Gl261 cells were cultivated in DMEM/F12 media with 4.5 g/liter glucose (Corning) supplemented with 10% FBS (Sigma-Aldrich) and no antibiotics at 37°C and 5% CO2 in a humidified atmosphere. All cell lines were tested to be mycoplasma free before any tumor implantation studies.

METHOD DETAILS

Murine Experimental Tumor Models—For orthotopic pancreatic tumor model, mice were anesthetized by inhalation of 2.5% isoflurane in 2% oxygen. An incision was made on the left side of the mouse to exteriorize the pancreas. 100×10^3 syngeneic PDAC cells in 10 μL PBS/Matrigel (Corning; vol/vol, 1:1) were injected into the pancreas using a Hamilton syringe. Injection point was sealed with tissue adhesive (3M Science) and allowed to dry for a few seconds. The incision was closed with discontinuous stitches using 6–0 polyglycolic acid clear sutures (Ethicon). Each mouse received 25 μg of buprenorphine post-operatively to alleviate pain. Mice were sacrificed 4–5 weeks post tumor implantation. For subcutaneous pancreatic tumor model, mice were anesthetized by inhalation of 2.5% isoflurane in oxygen. A flap of skin was lifted with forceps and 50×10^3 syngeneic PDAC cells in 100 μL PBS were injected into the skin using an insulin syringe. Tumor volume was calculated as length × width × width/2 in cubic millimeters.

For orthotopic GBM tumor model, a customized stereotactic setup with a guide-screw system was used for intracranial injection. Mice were anesthetized with ketamine and 20×10^3 syngeneic Gl261 cells in 5 μL cell media were stereo tactically injected into the brain with a Hamilton syringe. Mice were sacrificed ~3 weeks post tumor implantation. Tumor growth was measured with *in vivo* bioluminescent imaging one day post tumor implantation surgery on IVIS Lumina (PerkinElmer). Mice were anesthetized by inhalation

of 2% isoflurane in oxygen during the duration of the imaging. Exactly 15' prior to imaging, 200 μL of 15 mg/mL D-Luciferin solution (GoldBio) was intraperitoneally injected into each mouse and moved into the imaging chamber. Luminescence was used to measure tumor size (photons/s) of all genotypes at all time-points and analyzed simultaneously with Aura Imaging Software (Spectral Imaging Systems). At endpoint, reflex score was determined through toe pinch test (2 points for prompt withdrawal, 1 point for sluggish withdrawal and 0 points for no withdrawal of foot; calculated for each side). Presence of seizures at the time of sacrifice was noted as frequent rhythmic movement of forelimbs and/or whole body.

Mice of all genotypes were implanted with tumors in a randomized manner in all models.

Antibiotic treatment—All antibiotics were supplied ad libitum in drinking water in combination or alone comprising of ampicillin (1 g/L), vancomycin (0.5 g/L), neomycin (0.5 g/L), metronidazole (1 g/L) and amphotericin B (0.5 mg/L). Antibiotic treatment was performed for two weeks in experiments without tumors and for 5 weeks in experiments with tumors. Untreated mice were supplied with autoclaved water for the duration of the experiment.

Parabiosis—Surgical procedure was adapted from published protocol.[81] Only female littermates who were age and weight-matched were used. Each pair was independently co-housed for at least a week prior to procedure. On the day of surgery, mice were anesthetized by inhalation of 1.5% isoflurane in 2% oxygen and placed on heating pads during the entire procedure. Opposite lateral sides were shaved on each mouse within a pair, followed by matching skin incisions and separation of fascia along the elbow and knee joints without breaching the peritoneal cavities. Opposite olecranon and knee joints were aligned in a bent position and joined with non-absorbable 4–0 nylon sutures in triple surgical knots. Following the attachment of the joints, the ventral and dorsal skin of both mice was joined with discontinuous absorbable 6–0 PDS monofilament sutures. During the procedure each mouse was subcutaneously administered with 0.5 mL of 0.9% NaCl solution to prevent dehydration. Mice were allowed to recover on heated pads. Each mouse received 25 μg of buprenorphine S.R. and 0.5 mL of 0.9% NaCl solution post-op every 24h for 3 consecutive days to alleviate pain. Additionally, mice received two weeks of post-operative Baytril (0.175 mg/mL) antibiotic treatment in drinking water to prevent infections. Successful parabiotic pairs were classified as surviving healthy pairs two weeks after surgery.

Proliferation Assay—$KPC^{Il17ra+/+}$ and $KPC^{Il17ra-/-}$ cells were synchronized 48 hours before assay. After 48 hours, cells were plated in a 96-well flat bottom plate at 2500 cells/well in 20 technical replicates. Cell growth was monitored for 120 hours and analyzed by the IncuCyte Live-cell analysis imaging system. Log phase of growth curve was used to calculate doubling time.

***In vivo* antibody treatment—**Treatment was started 10 days after tumor implantation and after confirmation of palpable tumors. Each mouse was administered with matched vehicle, 100 μg of anti-CD20 (BioXCell), 200 μg of anti-IL-17RA (Amgen) or 200 μg of anti-IL-17 (Amgen) antibodies intraperitonially twice a week as indicated in experimental outline.

Histological Analysis—FFPE blocks were serially cut at 5 μm thickness. Slides were deparaffinized, rehydrated and stained with Hematoxylin and eosin. All bright field scans were obtained at 20X with Aperio Slide Scanner (Leica Biosystems).

Immunohistochemistry—FFPE tissue sections were deparaffinized, rehydrated in gradient alcohols. Antigen retrieval was performed with 1X Citrate buffer, pH 6.0 for 15’ at 99°C. Endogenous peroxidases were blocked with 0.3% H_2O_2 for 10’ at RT. Nonspecific epitopes were blocked with 2.5% normal goat serum (Vector Laboratories) for 45’. Primary antibody was incubated overnight at 4°C. Secondary ImmPRESS IgG antibody (Vector Laboratories) was used for 30’ at RT. Chromogenic substrate detection was done with SignalStain DAB (diaminobenzidine) Kit (Cell Signaling Technology) according to manufacturer’s instructions. Slides were counterstained with hematoxylin (Dako, Agilent) mounted in Acrymount (StatLab), and scanned at 20X with Aperio Scanscope Scanner (Leica Biosystems).

***In situ* hybridization—**Probes against mouse *Il17a* and *Il17f* were used according to manufacturer’s instructions (Advanced Cell Diagnostics). Opal detection system (Akoya Biosciences) was used for fluorescent HRP detection. Slides were imaged using the Vectra 3.0 spectral imaging system (PerkinElmer).

Sample preparation for immunoprofiling—Tumors were injected with 3 mL of tumor digestion buffer (1 mg/mL Collagenase P, 0.5 mg/mL DNAse I in HBSS) using an insulin syringe and topped up with another 3 mL of tumor digestion buffer and incubated for 10’ at 37°C. Digestion was stopped with 10% FBS HBSS media and filtered through 40 μm cell strainer. Next, tumors were incubated with Trypsin solution (1:4 0.25% Trypsin EDTA in HBSS) for 3’ at 37°C. At the end of the incubation, samples were washed with 10% FBS HBSS media.

Lamina propria isolation was adapted as previously reported.[59] Briefly ~3 cm of terminal ileum was harvested, Peyer’s patches were carefully excised, fat gently removed, followed by squeezing out of fecal material and flushed with PBS with an 18G needle. Next the tissue was opened longitudinally and cut into smaller pieces of ~0.5 cm and incubated with prewarmed EDTA buffer (10 μM EDTA, 10 μM HEPES in HBSS) at 37°C for 15’ with slow rotation. Next the tubes were placed on ice for an additional 15’. Tissues pieces were vigorously shaken and passed through a 100 μm cell strainer and rinsed several times with HBSS. Subsequently, 10 mL of prewarmed digestion buffer (0.5 mg/mL Collagenase D, 10 mg/mL DNAse I in HBSS, with Ca^{2+} & Mg^{2+}) was added and tissues pieces minced with sharp scissors. Samples were incubated at 37°C for 45’ with slow rotation. Tissues were vortexed intensely and passed through a 70 μm cell strainer and inactivated with 6 mL 10% FBS HBSS media and washed.

Spleen were incubated with High-Yield Lyse solution (Invitrogen) for 8’ at RT for erythrocyte removal. Lysis was stopped by adding cold HBSS and washed. Samples were filtered through 40 μm cell strainer before use.

Ileac Peyer's Patches, mesenteric and pancreatic lymph nodes were disintegrated with the back of a syringe plunger and passed through 40 μm cell strainer before use.

Flow cytometry—Samples were stained for viability with LIVE/DEAD Blue dye (Invitrogen), quenched with Fc block (BD Biosciences) diluted in FACS buffer (4% FBS, 100 μM EDTA in PBS) for another 10', RT. Surface antibody incubation was done at 1 μL/tube diluted in FACS buffer for 30' in dark at RT. Next samples were washed twice and fixed with CytoFix/CytoPerm buffer (BD Biosciences) for 20' in dark at 4°C. Sample acquisition was performed on LSRFortessa X-20 Cell Analyzer (BD Biosciences). Analysis was performed with FlowJo version 10.8.1 software. Antibody details including final concentrations can be found in STAR Resources.

Mass of cytometry (CyTOF)—Staining was performed as previously reported.[82] Samples were stained for viability with Cell-ID Cisplatin (Fluidigm) and washed with Maxpar Cell Staining buffer (Fluidgm). Next samples were incubated with Fc block (BD Biosciences), followed by incubation with surface antibody cocktail for 30' at RT. Samples were washed twice and fixed with CytoFix/CytoPerm buffer (BD Biosciences) for 20' in dark at 4°C and subsequently, barcoded using the Cell-ID 20-Plex Pd Barcodes (Fluidigm) for 30' at RT. Samples were then incubated with intracellular antibody cocktail for 45' at RT, washed twice and stained with Cell-ID Intercalator-Ir (Fluidigm) overnight. Sample acquisition was performed on Helios mass cytometer (Fluidigm). Raw data was debarcoded and preprocessed in FlowJo version 10.8.1 software to gate on Iridium stained, live cells. Further analysis was performed with RStudio as previously described.[83] Antibody details be found in Table S3.

Bulk RNA-seq and Analysis—Total RNA was extracted from fresh-frozen tumors and ~1cm of terminal ileum according to manufacturer's protocol (Qiagen). RNA integrity was confirmed on RNA Nano or Pico 6000 Bioanalyzer (Agilent Technologies). Libraries were prepared using Illumina TrueSeq Stranded Total RNA kit and sequenced on Illumina NextSeq 2000 System. Paired-end reads were aligned with University of California Santa Cruz Banana Slug Analytics Platform.

Significantly upregulated and downregulated genes were used as input for Interpretative phenomenological analysis (IPA) (Qiagen) and subsequently, only z scores with −log10 p value ≥ 1.3 were used for further analyses. For comparative analysis, all genes after comparison to samples from control mice with $p<0.1$ were used to identify common genes in ilea samples of mice with PDAC and GBM tumors. Gene Ontology (GO) analysis was performed with commonly downregulated genes in both groups.[84]

Single cell RNA-seq and Analysis—For single cell RNA sequencing library preparation, samples were prepared by Gel bead in emulsion (GEM) formed by oil micro-droplets, each containing a gel bead and a cell, by the Chromium instrument (10X Genomics). The reaction mixture/emulsion with captured and barcoded mRNAs were removed from the Chromium instrument followed by reverse transcription. The cDNA samples were fragmented and amplified per 10X protocol. The libraries were then purified, quantified, and sequenced on an Illumina NextSeq 550. Mapping of raw reads was

performed using the Cell Ranger pipeline (10X Genomics). Downstream analysis was done with Seurat package (V4.3.0) in R to generate UMAP from all the clusters identified in each sample type.[85] Significant differentially expressed genes in each cluster between the two comparison groups were identified using the *FindMarkers* function in Seurat R package, and input in clusterProfiler R package (V4.6.0) to identify differential pathways by GSEA analysis.[86] *FoldChange* function in Seurat R package was used to calculate average log2FC expression of *Il17a* and *Il17f* in indicated clusters between the groups.

Quantitative RT-PCR—Total RNA was extracted as described above and reverse transcribed with cDNA Reverse Transcription Kit (Applied Biosystems). Quantitative RT-PCR was performed in triplicates with Fast SYBR Green Master Mix (Applied Biosystems) on a ViiA 7 real-time PCR system (Applied Biosystems). Gene expression was normalized to *Gapdh* and ddCt was reported as fold change. All PCR primer sequences were obtained from Origene and validated on Primer-BLAST (NCBI) and manufactured through Integrated DNA Technologies (IDT).

Cytokine Detection—Whole blood was retro-orbitally collected in EDTA-coated tubes, plasma extracted and used undiluted for downstream assays. Cytokines were measured according to manufacturer's instructions.

Intracellular ROS production with Flow Cytometry—KPC cells treated with 50 ng/mL IL-17 *in vitro* for 7 days. After 7 days, cells were stained with CM-H_2DCFDA according to manufacturer's instructions. Sample acquisition was performed on LSRFortessa X-20 Cell Analyzer (BD Biosciences) in the 488 nm excitation channel. Analysis was performed with FlowJo version 10.8.1 software.

Extracellular ROS production using Amplex Red—KPC$^{Il17ra+/+}$ and KPC$^{Il17ra-/-}$ cells treated with 50 ng/ml IL-17 *in vitro* for 7 days. After 7 days, 500×10^6 cells were resuspended in 50 uL 1X Reaction buffer and then used for each replicate for measurement of H_2O_2 released by cells with Amplex Red Hydrogen Peroxidase kit according to manufacturer's instructions. Fluorescence was read at 530 nm excitation and 560 nm emission at each timepoint using a Biorad plate reader.

DNA extraction and bacterial 16S rRNA sequencing—16Sv4 rRNA gene sequencing methods were adapted from those developed for the NIH-Human Microbiome Project[87,88] and the Earth Microbiome Project.[89] Briefly, total genomic DNA was extracted using the Qiagen DNA extraction Kits for stool samples (DNeasy PowerSoil Pro Kit). The 16Sv4 rDNA region was amplified by PCR using the universal primers 515F and 806R and sequenced on the Illumina MiSeq platform using the 2×250 bp paired-end protocol. The primers used for amplification contain adapters for MiSeq sequencing and single-index barcodes so that the PCR products may be pooled and sequenced directly,[90] targeting at least 10,000 reads per sample. SFB detection in fecal DNA samples was performed as previously described.[59]

Microbiome Analysis Pipeline—Raw paired-end 16S rRNA reads (V4 region) were merged into consensus fragments by FLASH[91] and subsequently filtered for quality

(targeted error rate < 0.5%) and length (minimum 200bp) using Trimmomatic[92] and QIIME.[93,94] Spurious hits to the PhiX control genome were identified using BLASTN and removed. Passing sequences were trimmed of primers, evaluated for chimeras with UCLUST (de novo mode).[95] Chloroplast and mitochondrial contaminants were detected and filtered using the RDP classifier[96] with a confidence threshold of 50%. High-quality passing 16S rRNA sequences were assigned to a high-resolution taxonomic lineage using Resphera Insight[97,98] and SILVA Database v128.[99] Resulting contaminant-free 16S rRNA profiles were subsampled to 2,000 sequences per sample for downstream comparative analysis. Alpha- and beta-diversity analysis and principal coordinates analysis utilized QIIME and R. Differential abundance analysis of alpha diversity features of interest evaluated differences using the nonparametric difference test. Differential abundance analysis of taxonomic abundances evaluated differences using the negative binomial test (DESeq).[100] The false discovery rate (FDR) was used to correct for multiple hypothesis testing.[101] Generalized linear modeling adjusting for cohort membership and survival status was performed using R. Statistical annotations are added to denote significant correlations with metadata, enabling quick assessment of many variables.

CosMx Spatial Molecular Imaging (SMI)—CosMx SMI platform (NanoString Technologies Inc.) was used with three FFPE PDAC specimens as previously described.[102] Cellular phenotyping was performed using reference cellular profiles of human pancreas.[103] Cell assignments were verified using comparison to known marker gene expression, protein expression, and location within tissue. *IL17A* spatial cellular distribution was visualized with Napari software (NanoString Technologies Inc.). *IL17A* expression by cell type was reported as average normalized counts per cluster.

TCGA Analysis—Only TCGA PDAC patients were used for analysis. Patients were stratified as low or high for *IL17A* expression based on mean expression and then evaluated for *DUOX2* expression (UQ FPKM). For *DUOX2* high vs. low comparison, patients were stratified based on average expression and differentially expressed genes were extracted. Following this all the mapped significantly upregulated and downregulated genes were input into GSEA analysis to calculate enriched pathways.

QUANTIFICATION AND STATISTICAL ANALYSIS

Data were expressed as the mean ± SEM. Data were analyzed using GraphPad Prism 9.0 software (GraphPad Software, Inc.). Statistical significance between two groups was assessed using two-tailed student's t test for parametric and non-parametric testing depending on data distribution. When one variable was compared in more than two groups, one-way ANOVA was employed with Fisher's test. When two or more variables were compared in more than two groups, two-way ANOVA was employed with Fisher's test. Asterisks denoting the following values were as considered statistically significant: *P < 0.05, **P < 0.01, ***P < 0.001, or ****P < 0.0001.

Supplementary Material

Refer to Web version on PubMed Central for supplementary material.

Acknowledgments

Monoclonal neutralizing antibodies against IL-17RA was generously provided by Amgen. Dr. F. McAllister receives support from the National Cancer Institute (1R37CA237384), Cancer Prevention Research Institute of Texas (RP200173), V Foundation (Translational Award), Sabin Family Foundation, and Shelby-Lavine Pancreatic Scholars Program. V. Chandra received support from T32 Training Grant in Cancer Biology, University of Texas MD Anderson Cancer Center. Authors thank Dr. Drew Pardoll for helpful discussions during manuscript development. The graphical abstract was created with BioRender.com.

REFERENCES

1. Goldszmid RS, Dzutsev A, and Trinchieri G (2014). Host immune response to infection and cancer: unexpected commonalities. Cell Host Microbe 15, 295–305. 10.1016/j.chom.2014.02.003. [PubMed: 24629336]
2. Belkaid Y, and Hand TW (2014). Role of the microbiota in immunity and inflammation. Cell 157, 121–141. 10.1016/j.cell.2014.03.011. [PubMed: 24679531]
3. Ivanov II, Atarashi K, Manel N, Brodie EL, Shima T, Karaoz U, Wei D, Goldfarb KC, Santee CA, Lynch SV, et al. (2009). Induction of intestinal Th17 cells by segmented filamentous bacteria. Cell 139, 485–498. 10.1016/j.cell.2009.09.033. [PubMed: 19836068]
4. Conti HR, Shen F, Nayyar N, Stocum E, Sun JN, Lindemann MJ, Ho AW, Hai JH, Yu JJ, Jung JW, et al. (2009). Th17 cells and IL-17 receptor signaling are essential for mucosal host defense against oral candidiasis. J Exp Med 206, 299–311. 10.1084/jem.20081463. [PubMed: 19204111]
5. Amatya N, Garg AV, and Gaffen SL (2017). IL-17 Signaling: The Yin and the Yang. Trends Immunol 38, 310–322. 10.1016/j.it.2017.01.006. [PubMed: 28254169]
6. Toy D, Kugler D, Wolfson M, Vanden Bos T, Gurgel J, Derry J, Tocker J, and Peschon J (2006). Cutting edge: interleukin 17 signals through a heteromeric receptor complex. J Immunol 177, 36–39. 10.4049/jimmunol.177.1.36. [PubMed: 16785495]
7. Liang SC, Long AJ, Bennett F, Whitters MJ, Karim R, Collins M, Goldman SJ, Dunussi-Joannopoulos K, Williams CM, Wright JF, and Fouser LA (2007). An IL-17F/A heterodimer protein is produced by mouse Th17 cells and induces airway neutrophil recruitment. J Immunol 179, 7791–7799. 10.4049/jimmunol.179.11.7791. [PubMed: 18025225]
8. Wright JF, Guo Y, Quazi A, Luxenberg DP, Bennett F, Ross JF, Qiu Y, Whitters MJ, Tomkinson KN, Dunussi-Joannopoulos K, et al. (2007). Identification of an interleukin 17F/17A heterodimer in activated human CD4+ T cells. J Biol Chem 282, 13447–13455. 10.1074/jbc.M700499200. [PubMed: 17355969]
9. Rickel EA, Siegel LA, Yoon BR, Rottman JB, Kugler DG, Swart DA, Anders PM, Tocker JE, Comeau MR, and Budelsky AL (2008). Identification of functional roles for both IL-17RB and IL-17RA in mediating IL-25-induced activities. J Immunol 181, 4299–4310. 10.4049/jimmunol.181.6.4299. [PubMed: 18768888]
10. Ivanov II, McKenzie BS, Zhou L, Tadokoro CE, Lepelley A, Lafaille JJ, Cua DJ, and Littman DR (2006). The orphan nuclear receptor RORgammat directs the differentiation program of proinflammatory IL-17+ T helper cells. Cell 126, 1121–1133. 10.1016/j.cell.2006.07.035. [PubMed: 16990136]
11. Intlekofer AM, Banerjee A, Takemoto N, Gordon SM, Dejong CS, Shin H, Hunter CA, Wherry EJ, Lindsten T, and Reiner SL (2008). Anomalous type 17 response to viral infection by CD8+ T cells lacking T-bet and eomesodermin. Science 321, 408–411. 10.1126/science.1159806. [PubMed: 18635804]
12. Lockhart E, Green AM, and Flynn JL (2006). IL-17 production is dominated by gammadelta T cells rather than CD4 T cells during Mycobacterium tuberculosis infection. J Immunol 177, 4662–4669. 10.4049/jimmunol.177.7.4662. [PubMed: 16982905]
13. Takatori H, Kanno Y, Watford WT, Tato CM, Weiss G, Ivanov II, Littman DR, and O'Shea JJ (2009). Lymphoid tissue inducer-like cells are an innate source of IL-17 and IL-22. J Exp Med 206, 35–41. 10.1084/jem.20072713. [PubMed: 19114665]
14. Cua DJ, and Tato CM (2010). Innate IL-17-producing cells: the sentinels of the immune system. Nat Rev Immunol 10, 479–489. 10.1038/nri2800. [PubMed: 20559326]

15. Yang XP, Ghoreschi K, Steward-Tharp SM, Rodriguez-Canales J, Zhu J, Grainger JR, Hirahara K, Sun HW, Wei L, Vahedi G, et al. (2011). Opposing regulation of the locus encoding IL-17 through direct, reciprocal actions of STAT3 and STAT5. Nat Immunol 12, 247–254. 10.1038/ni.1995. [PubMed: 21278738]

16. Zhang F, Meng G, and Strober W (2008). Interactions among the transcription factors Runx1, RORgammat and Foxp3 regulate the differentiation of interleukin 17-producing T cells. Nat Immunol 9, 1297–1306. 10.1038/ni.1663. [PubMed: 18849990]

17. Ishigame H, Kakuta S, Nagai T, Kadoki M, Nambu A, Komiyama Y, Fujikado N, Tanahashi Y, Akitsu A, Kotaki H, et al. (2009). Differential roles of interleukin-17A and −17F in host defense against mucoepithelial bacterial infection and allergic responses. Immunity 30, 108–119. 10.1016/j.immuni.2008.11.009. [PubMed: 19144317]

18. Song X, Gao H, Lin Y, Yao Y, Zhu S, Wang J, Liu Y, Yao X, Meng G, Shen N, et al. (2014). Alterations in the microbiota drive interleukin-17C production from intestinal epithelial cells to promote tumorigenesis. Immunity 40, 140–152. 10.1016/j.immuni.2013.11.018. [PubMed: 24412611]

19. Takahashi N, Vanlaere I, de Rycke R, Cauwels A, Joosten LA, Lubberts E, van den Berg WB, and Libert C (2008). IL-17 produced by Paneth cells drives TNF-induced shock. J Exp Med 205, 1755–1761. 10.1084/jem.20080588. [PubMed: 18663129]

20. Yao ZB, Fanslow WC, Seldin MF, Rousseau AM, Painter SL, Comeau MR, Cohen JI, and Spriggs MK (1995). Herpesvirus Saimiri encodes a new cytokine, IL-17, which binds to a novel cytokine receptor. Immunity 3, 811–821. Doi 10.1016/1074-7613(95)90070-5. [PubMed: 8777726]

21. Uhlen M, Fagerberg L, Hallstrom BM, Lindskog C, Oksvold P, Mardinoglu A, Sivertsson A, Kampf C, Sjostedt E, Asplund A, et al. (2015). Proteomics. Tissue-based map of the human proteome. Science 347, 1260419. 10.1126/science.1260419. [PubMed: 25613900]

22. Chiricozzi A, Guttman-Yassky E, Suarez-Farinas M, Nograles KE, Tian S, Cardinale I, Chimenti S, and Krueger JG (2011). Integrative responses to IL-17 and TNF-alpha in human keratinocytes account for key inflammatory pathogenic circuits in psoriasis. J Invest Dermatol 131, 677–687. 10.1038/jid.2010.340. [PubMed: 21085185]

23. Kotake S, Udagawa N, Takahashi N, Matsuzaki K, Itoh K, Ishiyama S, Saito S, Inoue K, Kamatani N, Gillespie MT, et al. (1999). IL-17 in synovial fluids from patients with rheumatoid arthritis is a potent stimulator of osteoclastogenesis. J Clin Invest 103, 1345–1352. 10.1172/JCI5703. [PubMed: 10225978]

24. Wong CK, Lit LC, Tam LS, Li EK, Wong PT, and Lam CW (2008). Hyperproduction of IL-23 and IL-17 in patients with systemic lupus erythematosus: implications for Th17-mediated inflammation in auto-immunity. Clin Immunol 127, 385–393. 10.1016/j.clim.2008.01.019. [PubMed: 18373953]

25. Fujino S, Andoh A, Bamba S, Ogawa A, Hata K, Araki Y, Bamba T, and Fujiyama Y (2003). Increased expression of interleukin 17 in inflammatory bowel disease. Gut 52, 65–70. 10.1136/gut.52.1.65. [PubMed: 12477762]

26. Lock C, Hermans G, Pedotti R, Brendolan A, Schadt E, Garren H, Langer-Gould A, Strober S, Cannella B, Allard J, et al. (2002). Gene-microarray analysis of multiple sclerosis lesions yields new targets validated in autoimmune encephalomyelitis. Nat Med 8, 500–508. 10.1038/nm0502-500. [PubMed: 11984595]

27. McAllister F, Bailey JM, Alsina J, Nirschl CJ, Sharma R, Fan H, Rattigan Y, Roeser JC, Lankapalli RH, Zhang H, et al. (2014). Oncogenic Kras activates a hematopoietic-to-epithelial IL-17 signaling axis in preinvasive pancreatic neoplasia. Cancer Cell 25, 621–637. 10.1016/j.ccr.2014.03.014. [PubMed: 24823639]

28. Loncle C, Bonjoch L, Folch-Puy E, Lopez-Millan MB, Lac S, Molejon MI, Chuluyan E, Cordelier P, Dubus P, Lomberk G, et al. (2015). IL17 Functions through the Novel REG3beta-JAK2-STAT3 Inflammatory Pathway to Promote the Transition from Chronic Pancreatitis to Pancreatic Cancer. Cancer Res 75, 4852–4862. 10.1158/0008-5472.CAN-15-0896. [PubMed: 26404002]

29. Zhang Y, Zoltan M, Riquelme E, Xu H, Sahin I, Castro-Pando S, Montiel MF, Chang K, Jiang Z, Ling J, et al. (2018). Immune Cell Production of Interleukin 17 Induces Stem Cell Features of Pancreatic Intraepithelial Neoplasia Cells. Gastroenterology 155, 210–223 e213. 10.1053/j.gastro.2018.03.041. [PubMed: 29604293]

30. Zhang Y, Chandra V, Riquelme Sanchez E, Dutta P, Quesada PR, Rakoski A, Zoltan M, Arora N, Baydogan S, Horne W, et al. (2020). Interleukin-17-induced neutrophil extracellular traps mediate resistance to checkpoint blockade in pancreatic cancer. J Exp Med 217. 10.1084/jem.20190354.

31. Mucciolo G, Curcio C, Roux C, Li WY, Capello M, Curto R, Chiarle R, Giordano D, Satolli MA, Lawlor R, et al. (2021). IL17A critically shapes the transcriptional program of fibroblasts in pancreatic cancer and switches on their protumorigenic functions. Proc Natl Acad Sci U S A 118. 10.1073/pnas.2020395118.

32. Alinejad V, Dolati S, Motallebnezhad M, and Yousefi M (2017). The role of IL17B-IL17RB signaling pathway in breast cancer. Biomed Pharmacother 88, 795–803. 10.1016/j.biopha.2017.01.120. [PubMed: 28160754]

33. Sinha VC, Rinkenbaugh AL, Xu M, Zhou X, Zhang X, Jeter-Jones S, Shao J, Qi Y, Zebala JA, Maeda DY, et al. (2021). Single-cell evaluation reveals shifts in the tumor-immune niches that shape and maintain aggressive lesions in the breast. Nat Commun 12, 5024. 10.1038/s41467-021-25240-z. [PubMed: 34408137]

34. Ma HY, Yamamoto G, Xu J, Liu X, Karin D, Kim JY, Alexandrov LB, Koyama Y, Nishio T, Benner C, et al. (2020). IL-17 signaling in steatotic hepatocytes and macrophages promotes hepatocellular carcinoma in alcohol-related liver disease. J Hepatol 72, 946–959. 10.1016/j.jhep.2019.12.016. [PubMed: 31899206]

35. Numasaki M, Watanabe M, Suzuki T, Takahashi H, Nakamura A, McAllister F, Hishinuma T, Goto J, Lotze MT, Kolls JK, and Sasaki H (2005). IL-17 enhances the net angiogenic activity and in vivo growth of human non-small cell lung cancer in SCID mice through promoting CXCR-2-dependent angiogenesis. J Immunol 175, 6177–6189. 10.4049/jimmunol.175.9.6177. [PubMed: 16237115]

36. Chang SH, Mirabolfathinejad SG, Katta H, Cumpian AM, Gong L, Caetano MS, Moghaddam SJ, and Dong C (2014). T helper 17 cells play a critical pathogenic role in lung cancer. Proc Natl Acad Sci U S A 111, 5664–5669. 10.1073/pnas.1319051111. [PubMed: 24706787]

37. Wu S, Rhee KJ, Albesiano E, Rabizadeh S, Wu X, Yen HR, Huso DL, Brancati FL, Wick E, McAllister F, et al. (2009). A human colonic commensal promotes colon tumorigenesis via activation of T helper type 17 T cell responses. Nat Med 15, 1016–1022. 10.1038/nm.2015. [PubMed: 19701202]

38. Wang K, Kim MK, Di Caro G, Wong J, Shalapour S, Wan J, Zhang W, Zhong Z, Sanchez-Lopez E, Wu LW, et al. (2014). Interleukin-17 receptor a signaling in transformed enterocytes promotes early colorectal tumorigenesis. Immunity 41, 1052–1063. 10.1016/j.immuni.2014.11.009. [PubMed: 25526314]

39. Numasaki M, Fukushi J, Ono M, Narula SK, Zavodny PJ, Kudo T, Robbins PD, Tahara H, and Lotze MT (2003). Interleukin-17 promotes angiogenesis and tumor growth. Blood 101, 2620–2627. 10.1182/blood-2002-05-1461. [PubMed: 12411307]

40. Cantini G, Pisati F, Mastropietro A, Frattini V, Iwakura Y, Finocchiaro G, and Pellegatta S (2011). A critical role for regulatory T cells in driving cytokine profiles of Th17 cells and their modulation of glioma microenvironment. Cancer Immunol Immunother 60, 1739–1750. 10.1007/s00262-011-1069-4. [PubMed: 21779877]

41. Housseau F, Wu S, Wick EC, Fan H, Wu X, Llosa NJ, Smith KN, Tam A, Ganguly S, Wanyiri JW, et al. (2016). Redundant Innate and Adaptive Sources of IL17 Production Drive Colon Tumorigenesis. Cancer Res 76, 2115–2124. 10.1158/0008-5472.CAN-15-0749. [PubMed: 26880802]

42. Kryczek I, Banerjee M, Cheng P, Vatan L, Szeliga W, Wei S, Huang E, Finlayson E, Simeone D, Welling TH, et al. (2009). Phenotype, distribution, generation, and functional and clinical relevance of Th17 cells in the human tumor environments. Blood 114, 1141–1149. 10.1182/blood-2009-03-208249. [PubMed: 19470694]

43. Muranski P, Boni A, Antony PA, Cassard L, Irvine KR, Kaiser A, Paulos CM, Palmer DC, Touloukian CE, Ptak K, et al. (2008). Tumor-specific Th17-polarized cells eradicate large established melanoma. Blood 112, 362–373. 10.1182/blood-2007-11-120998. [PubMed: 18354038]

44. Martin-Orozco N, Muranski P, Chung Y, Yang XO, Yamazaki T, Lu S, Hwu P, Restifo NP, Overwijk WW, and Dong C (2009). T helper 17 cells promote cytotoxic T cell activation in tumor immunity. Immunity 31, 787–798. 10.1016/j.immuni.2009.09.014. [PubMed: 19879162]
45. Kim BS, Kuen DS, Koh CH, Kim HD, Chang SH, Kim S, Jeon YK, Park YJ, Choi G, Kim J, et al. (2021). Type 17 immunity promotes the exhaustion of CD8(+) T cells in cancer. J Immunother Cancer 9. 10.1136/jitc-2021-002603.
46. Briukhovetska D, Dorr J, Endres S, Libby P, Dinarello CA, and Kobold S (2021). Interleukins in cancer: from biology to therapy. Nat Rev Cancer 21, 481–499. 10.1038/s41568-021-00363-z. [PubMed: 34083781]
47. Bilal J, Berlinberg A, Riaz IB, Faridi W, Bhattacharjee S, Ortega G, Murad MH, Wang Z, Prokop LJ, Alhifany AA, and Kwoh CK (2019). Risk of Infections and Cancer in Patients With Rheumatologic Diseases Receiving Interleukin Inhibitors: A Systematic Review and Meta-analysis. JAMA Netw Open 2, e1913102. 10.1001/jamanetworkopen.2019.13102. [PubMed: 31626313]
48. Sepich-Poore GD, Zitvogel L, Straussman R, Hasty J, Wargo JA, and Knight R (2021). The microbiome and human cancer. Science 371. 10.1126/science.abc4552.
49. Chandra V, and McAllister F (2021). Therapeutic potential of microbial modulation in pancreatic cancer. Gut. 10.1136/gutjnl-2019-319807.
50. Geller LT, Barzily-Rokni M, Danino T, Jonas OH, Shental N, Nejman D, Gavert N, Zwang Y, Cooper ZA, Shee K, et al. (2017). Potential role of intratumor bacteria in mediating tumor resistance to the chemotherapeutic drug gemcitabine. Science 357, 1156–1160. 10.1126/science.aah5043. [PubMed: 28912244]
51. Riquelme E, Zhang Y, Zhang L, Montiel M, Zoltan M, Dong W, Quesada P, Sahin I, Chandra V, San Lucas A, et al. (2019). Tumor Microbiome Diversity and Composition Influence Pancreatic Cancer Outcomes. Cell 178, 795–806 e712. 10.1016/j.cell.2019.07.008. [PubMed: 31398337]
52. Mendez R, Kesh K, Arora N, Di Martino L, McAllister F, Merchant N, Banerjee S, and Banerjee S (2019). Microbial dysbiosis and polyamine metabolism as predictive markers for early detection of pancreatic cancer. Carcinogenesis. 10.1093/carcin/bgz116.
53. Sethi V, Kurtom S, Tarique M, Lavania S, Malchiodi Z, Hellmund L, Zhang L, Sharma U, Giri B, Garg B, et al. (2018). Gut Microbiota Promotes Tumor Growth in Mice by Modulating Immune Response. Gastroenterology 155, 33–37 e36. 10.1053/j.gastro.2018.04.001. [PubMed: 29630898]
54. Pushalkar S, Hundeyin M, Daley D, Zambirinis CP, Kurz E, Mishra A, Mohan N, Aykut B, Usyk M, Torres LE, et al. (2018). The Pancreatic Cancer Microbiome Promotes Oncogenesis by Induction of Innate and Adaptive Immune Suppression. Cancer Discov 8, 403–416. 10.1158/2159-8290.CD-17-1134. [PubMed: 29567829]
55. Thomas RM, Gharaibeh RZ, Gauthier J, Beveridge M, Pope JL, Guijarro MV, Yu Q, He Z, Ohland C, Newsome R, et al. (2018). Intestinal microbiota enhances pancreatic carcinogenesis in preclinical models. Carcinogenesis 39, 1068–1078. 10.1093/carcin/bgy073. [PubMed: 29846515]
56. Imai H, Saijo K, Komine K, Otsuki Y, Ohuchi K, Sato Y, Okita A, Takahashi M, Takahashi S, Shirota H, et al. (2019). Antibiotic therapy augments the efficacy of gemcitabine-containing regimens for advanced cancer: a retrospective study. Cancer Manag Res 11, 7953–7965. 10.2147/CMAR.S215697. [PubMed: 31686910]
57. Nakano S, Komatsu Y, Kawamoto Y, Saito R, Ito K, Nakatsumi H, Yuki S, and Sakamoto N (2020). Association between the use of antibiotics and efficacy of gemcitabine plus nab-paclitaxel in advanced pancreatic cancer. Medicine (Baltimore) 99, e22250. 10.1097/MD.0000000000022250. [PubMed: 32991420]
58. Mohindroo C, Hasanov M, Rogers JE, Dong W, Prakash LR, Baydogan S, Mizrahi JD, Overman MJ, Varadhachary GR, Wolff RA, et al. (2021). Antibiotic use influences outcomes in advanced pancreatic adenocarcinoma patients. Cancer Med 10, 5041–5050. 10.1002/cam4.3870. [PubMed: 34250759]
59. Kumar P, Monin L, Castillo P, Elsegeiny W, Horne W, Eddens T, Vikram A, Good M, Schoenborn AA, Bibby K, et al. (2016). Intestinal Interleukin-17 Receptor Signaling Mediates Reciprocal Control of the Gut Microbiota and Autoimmune Inflammation. Immunity 44, 659–671. 10.1016/j.immuni.2016.02.007. [PubMed: 26982366]

60. Lin X, Gaudino SJ, Jang KK, Bahadur T, Singh A, Banerjee A, Beaupre M, Chu T, Wong HT, Kim CK, et al. (2022). IL-17RA-signaling in Lgr5(+) intestinal stem cells induces expression of transcription factor ATOH1 to promote secretory cell lineage commitment. Immunity 55, 237–253 e238. 10.1016/j.immuni.2021.12.016. [PubMed: 35081371]

61. Huang Y, Tang J, Cai Z, Zhou K, Chang L, Bai Y, and Ma Y (2020). Prevotella Induces the Production of Th17 Cells in the Colon of Mice. J Immunol Res 2020, 9607328. 10.1155/2020/9607328. [PubMed: 33204736]

62. Regen T, Isaac S, Amorim A, Nunez NG, Hauptmann J, Shanmugavadivu A, Klein M, Sankowski R, Mufazalov IA, Yogev N, et al. (2021). IL-17 controls central nervous system autoimmunity through the intestinal microbiome. Sci Immunol 6. 10.1126/sciimmunol.aaz6563.

63. Wainwright DA, Sengupta S, Han Y, Ulasov IV, and Lesniak MS (2010). The presence of IL-17A and T helper 17 cells in experimental mouse brain tumors and human glioma. PLoS One 5, e15390. 10.1371/journal.pone.0015390. [PubMed: 21060663]

64. Mirlekar B, Wang Y, Li S, Zhou M, Entwistle S, De Buysscher T, Morrison A, Herrera G, Harris C, Vincent BG, et al. (2022). Balance between immunoregulatory B cells and plasma cells drives pancreatic tumor immunity. Cell Rep Med 3, 100744. 10.1016/j.xcrm.2022.100744. [PubMed: 36099917]

65. Matsunaga Y, Clark T, Wanek AG, Bitoun JP, Gong Q, Good M, and Kolls JK (2021). Intestinal IL-17R Signaling Controls Secretory IgA and Oxidase Balance in Citrobacter rodentium Infection. J Immunol 206, 766–775. 10.4049/jimmunol.2000591. [PubMed: 33431657]

66. Lam KC, Araya RE, Huang A, Chen Q, Di Modica M, Rodrigues RR, Lopes A, Johnson SB, Schwarz B, Bohrnsen E, et al. (2021). Microbiota triggers STING-type I IFN-dependent monocyte reprogramming of the tumor microenvironment. Cell 184, 5338–5356 e5321. 10.1016/j.cell.2021.09.019. [PubMed: 34624222]

67. Manasson J, Wallach DS, Guggino G, Stapylton M, Badri MH, Solomon G, Reddy SM, Coras R, Aksenov AA, Jones DR, et al. (2020). Interleukin-17 Inhibition in Spondyloarthritis Is Associated With Subclinical Gut Microbiome Perturbations and a Distinctive Interleukin-25-Driven Intestinal Inflammation. Arthritis Rheumatol 72, 645–657. 10.1002/art.41169. [PubMed: 31729183]

68. Half E, Keren N, Reshef L, Dorfman T, Lachter I, Kluger Y, Reshef N, Knobler H, Maor Y, Stein A, et al. (2019). Fecal microbiome signatures of pancreatic cancer patients. Sci Rep 9, 16801. 10.1038/s41598-019-53041-4. [PubMed: 31727922]

69. Kartal E, Schmidt TSB, Molina-Montes E, Rodriguez-Perales S, Wirbel J, Maistrenko OM, Akanni WA, Alashkar Alhamwe B, Alves RJ, Carrato A, et al. (2022). A faecal microbiota signature with high specificity for pancreatic cancer. Gut 71, 1359–1372. 10.1136/gutjnl-2021-324755. [PubMed: 35260444]

70. Mitsdoerffer M, Lee Y, Jager A, Kim HJ, Korn T, Kolls JK, Cantor H, Bettelli E, and Kuchroo VK (2010). Proinflammatory T helper type 17 cells are effective B-cell helpers. Proc Natl Acad Sci U S A 107, 14292–14297. 10.1073/pnas.1009234107. [PubMed: 20660725]

71. Pylayeva-Gupta Y, Das S, Handler JS, Hajdu CH, Coffre M, Koralov SB, and Bar-Sagi D (2016). IL35-Producing B Cells Promote the Development of Pancreatic Neoplasia. Cancer Discov 6, 247–255. 10.1158/2159-8290.CD-15-0843. [PubMed: 26715643]

72. Gunderson AJ, Kaneda MM, Tsujikawa T, Nguyen AV, Affara NI, Ruffell B, Gorjestani S, Liudahl SM, Truitt M, Olson P, et al. (2016). Bruton Tyrosine Kinase-Dependent Immune Cell Cross-talk Drives Pancreas Cancer. Cancer Discov 6, 270–285. 10.1158/2159-8290.CD-15-0827. [PubMed: 26715645]

73. Geiszt M, Witta J, Baffi J, Lekstrom K, and Leto TL (2003). Dual oxidases represent novel hydrogen peroxide sources supporting mucosal surface host defense. FASEB J 17, 1502–1504. 10.1096/fj.02-1104fje. [PubMed: 12824283]

74. Corcionivoschi N, Alvarez LA, Sharp TH, Strengert M, Alemka A, Mantell J, Verkade P, Knaus UG, and Bourke B (2012). Mucosal reactive oxygen species decrease virulence by disrupting Campylobacter jejuni phosphotyrosine signaling. Cell Host Microbe 12, 47–59. 10.1016/j.chom.2012.05.018. [PubMed: 22817987]

75. Haberman Y, Tickle TL, Dexheimer PJ, Kim MO, Tang D, Karns R, Baldassano RN, Noe JD, Rosh J, Markowitz J, et al. (2014). Pediatric Crohn disease patients exhibit specific ileal

transcriptome and microbiome signature. J Clin Invest 124, 3617–3633. 10.1172/JCI75436. [PubMed: 25003194]

76. Wu Y, Antony S, Juhasz A, Lu J, Ge Y, Jiang G, Roy K, and Doroshow JH (2011). Up-regulation and sustained activation of Stat1 are essential for interferon-gamma (IFN-gamma)-induced dual oxidase 2 (Duox2) and dual oxidase A2 (DuoxA2) expression in human pancreatic cancer cell lines. J Biol Chem 286, 12245–12256. 10.1074/jbc.M110.191031. [PubMed: 21321110]
77. Wang SL, Wu Y, Konate M, Lu J, Mallick D, Antony S, Meitzler JL, Jiang G, Dahan I, Juhasz A, et al. (2023). Exogenous DNA enhances DUOX2 expression and function in human pancreatic cancer cells by activating the cGAS-STING signaling pathway. Free Radic Biol Med 205, 262–274. 10.1016/j.freeradbiomed.2023.06.012. [PubMed: 37330147]
78. Lyu PW, Xu XD, Zong K, and Qiu XG (2022). Overexpression of DUOX2 mediates doxorubicin resistance and predicts prognosis of pancreatic cancer. Gland Surg 11, 115–124. 10.21037/gs-21-776. [PubMed: 35242674]
79. Hueber W, Sands BE, Lewitzky S, Vandemeulebroecke M, Reinisch W, Higgins PD, Wehkamp J, Feagan BG, Yao MD, Karczewski M, et al. (2012). Secukinumab, a human anti-IL-17A monoclonal antibody, for moderate to severe Crohn's disease: unexpected results of a randomised, double-blind placebo-controlled trial. Gut 61, 1693–1700. 10.1136/gutjnl-2011-301668. [PubMed: 22595313]
80. Targan SR, Feagan BG, Vermeire S, Panaccione R, Melmed GY, Blosch C, Newmark R, Zhang N, Chon Y, Lin SL, and Klekotka P (2012). A Randomized, Double-Blind, Placebo-Controlled Study to Evaluate the Safety, Tolerability, and Efficacy of AMG 827 in Subjects With Moderate to Severe Crohn's Disease. Gastroenterology 143, E26–E26. DOI 10.1053/j.gastro.2012.07.084.
81. Kamran P, Sereti KI, Zhao P, Ali SR, Weissman IL, and Ardehali R (2013). Parabiosis in mice: a detailed protocol. J Vis Exp. 10.3791/50556.
82. Chandra V, McAllister F, and Burks JK (2022). Cytometry of Mass for Murine Immunoprofiling. Methods Mol Biol 2435, 129–137. 10.1007/978-1-0716-2014-4_9. [PubMed: 34993943]
83. Nowicka M, Krieg C, Crowell HL, Weber LM, Hartmann FJ, Guglietta S, Becher B, Levesque MP, and Robinson MD (2017). CyTOF workflow: differential discovery in high-throughput high-dimensional cytometry datasets. F1000Res 6, 748. 10.12688/f1000research.11622.3. [PubMed: 28663787]
84. Mi H, Muruganujan A, Ebert D, Huang X, and Thomas PD (2019). PANTHER version 14: more genomes, a new PANTHER GO-slim and improvements in enrichment analysis tools. Nucleic Acids Res 47, D419–D426. 10.1093/nar/gky1038. [PubMed: 30407594]
85. Hao Y, Hao S, Andersen-Nissen E, Mauck WM 3rd, Zheng S, Butler A, Lee MJ, Wilk AJ, Darby C, Zager M, et al. (2021). Integrated analysis of multimodal single-cell data. Cell 184, 3573–3587 e3529. 10.1016/j.cell.2021.04.048. [PubMed: 34062119]
86. Wu T, Hu E, Xu S, Chen M, Guo P, Dai Z, Feng T, Zhou L, Tang W, Zhan L, et al. (2021). clusterProfiler 4.0: A universal enrichment tool for interpreting omics data. Innovation (Camb) 2, 100141. 10.1016/j.xinn.2021.100141. [PubMed: 34557778]
87. Human Microbiome Project C (2012). Structure, function and diversity of the healthy human microbiome. Nature 486, 207–214. 10.1038/nature11234. [PubMed: 22699609]
88. Human Microbiome Project C (2012). A framework for human microbiome research. Nature 486, 215–221. 10.1038/nature11209. [PubMed: 22699610]
89. Thompson LR, Sanders JG, McDonald D, Amir A, Ladau J, Locey KJ, Prill RJ, Tripathi A, Gibbons SM, Ackermann G, et al. (2017). A communal catalogue reveals Earth's multiscale microbial diversity. Nature 551, 457–463. 10.1038/nature24621. [PubMed: 29088705]
90. Caporaso JG, Lauber CL, Walters WA, Berg-Lyons D, Huntley J, Fierer N, Owens SM, Betley J, Fraser L, Bauer M, et al. (2012). Ultra-high-throughput microbial community analysis on the Illumina HiSeq and MiSeq platforms. ISME J 6, 1621–1624. 10.1038/ismej.2012.8. [PubMed: 22402401]
91. Magoc T, and Salzberg SL (2011). FLASH: fast length adjustment of short reads to improve genome assemblies. Bioinformatics 27, 2957–2963. 10.1093/bioinformatics/btr507. [PubMed: 21903629]

92. Bolger AM, Lohse M, and Usadel B (2014). Trimmomatic: a flexible trimmer for Illumina sequence data. Bioinformatics 30, 2114–2120. 10.1093/bioinformatics/btu170. [PubMed: 24695404]

93. Caporaso JG, Bittinger K, Bushman FD, DeSantis TZ, Andersen GL, and Knight R (2010). PyNAST: a flexible tool for aligning sequences to a template alignment. Bioinformatics 26, 266–267. 10.1093/bioinformatics/btp636. [PubMed: 19914921]

94. Kuczynski J, Stombaugh J, Walters WA, Gonzalez A, Caporaso JG, and Knight R (2011). Using QIIME to analyze 16S rRNA gene sequences from microbial communities. Curr Protoc Bioinformatics Chapter 10, 10 17 11–10 17 20. 10.1002/0471250953.bi1007s36.

95. Edgar RC, Haas BJ, Clemente JC, Quince C, and Knight R (2011). UCHIME improves sensitivity and speed of chimera detection. Bioinformatics 27, 2194–2200. 10.1093/bioinformatics/btr381. [PubMed: 21700674]

96. Wang Q, Garrity GM, Tiedje JM, and Cole JR (2007). Naive Bayesian classifier for rapid assignment of rRNA sequences into the new bacterial taxonomy. Appl Environ Microbiol 73, 5261–5267. 10.1128/AEM.00062-07. [PubMed: 17586664]

97. Daquigan N, Seekatz AM, Greathouse KL, Young VB, and White JR (2017). High-resolution profiling of the gut microbiome reveals the extent of Clostridium difficile burden. NPJ Biofilms Microbiomes 3, 35. 10.1038/s41522-017-0043-0. [PubMed: 29214047]

98. Drewes JL, White JR, Dejea CM, Fathi P, Iyadorai T, Vadivelu J, Roslani AC, Wick EC, Mongodin EF, Loke MF, et al. (2017). High-resolution bacterial 16S rRNA gene profile meta-analysis and biofilm status reveal common colorectal cancer consortia. NPJ Biofilms Microbiomes 3, 34. 10.1038/s41522-017-0040-3. [PubMed: 29214046]

99. Quast C, Pruesse E, Yilmaz P, Gerken J, Schweer T, Yarza P, Peplies J, and Glockner FO (2013). The SILVA ribosomal RNA gene database project: improved data processing and web-based tools. Nucleic Acids Res 41, D590–596. 10.1093/nar/gks1219. [PubMed: 23193283]

100. Anders S, and Huber W (2010). Differential expression analysis for sequence count data. Genome Biol 11, R106. 10.1186/gb-2010-11-10-r106. [PubMed: 20979621]

101. Benjamini Y, Drai D, Elmer G, Kafkafi N, and Golani I (2001). Controlling the false discovery rate in behavior genetics research. Behav Brain Res 125, 279–284. 10.1016/s0166-4328(01)00297-2. [PubMed: 11682119]

102. He S, Bhatt R, Brown C, Brown EA, Buhr DL, Chantranuvatana K, Danaher P, Dunaway D, Garrison RG, Geiss G, et al. (2022). High-plex imaging of RNA and proteins at subcellular resolution in fixed tissue by spatial molecular imaging. Nat Biotechnol 40, 1794–1806. 10.1038/s41587-022-01483-z. [PubMed: 36203011]

103. Enge M, Arda HE, Mignardi M, Beausang J, Bottino R, Kim SK, and Quake SR (2017). Single-Cell Analysis of Human Pancreas Reveals Transcriptional Signatures of Aging and Somatic Mutation Patterns. Cell 171, 321–330 e314. 10.1016/j.cell.2017.09.004. [PubMed: 28965763]

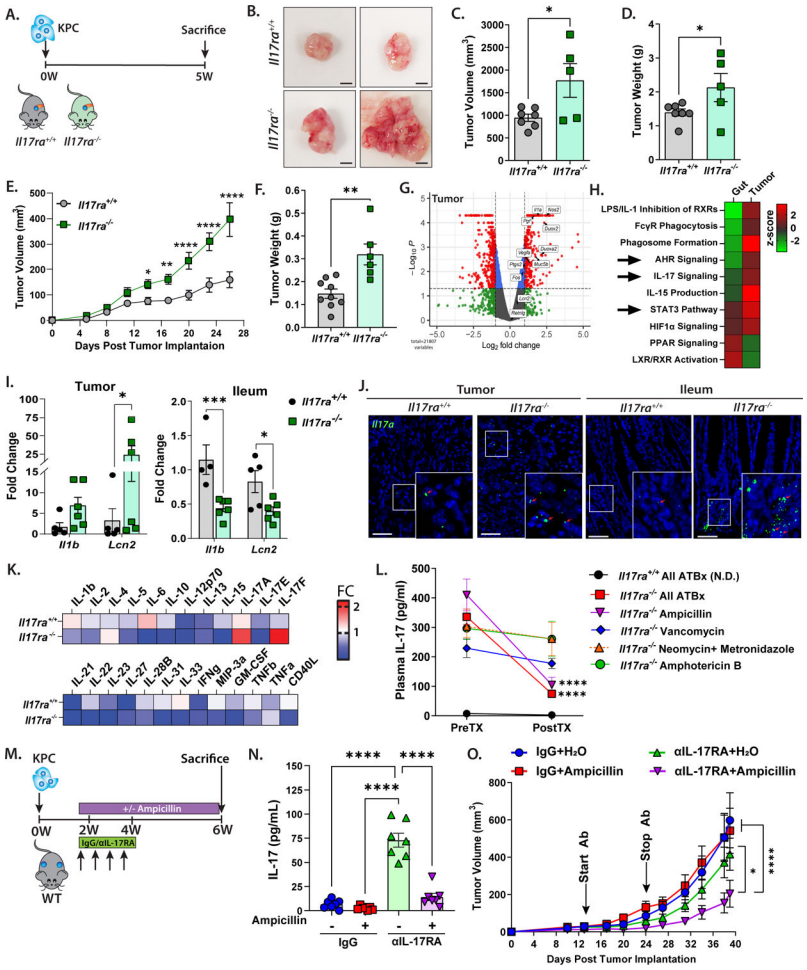

Figure 1: Microbially driven elevation of IL-17 promotes pancreatic tumor growth

A.Experimental outline of murine PDAC model. Pancreata (orthotopic) or skin (subcutaneous) of *Il17ra*$^{+/+}$ and *Il17ra*$^{-/-}$ mice were implanted with KPC cells and sacrificed after 4–5 weeks.

B. Representative images (duplicates) of PDAC orthotopic tumors from *Il17ra*$^{+/+}$ and *Il17ra*$^{-/-}$ mice at endpoint. Scale bar represents 3 mm.

C-D. Orthotopic tumor volumes (C) and weight (D) at endpoint.

E-F. Subcutaneous tumor growth curves (E) and end-point tumor weight (F).

G. Volcano plot showing upregulated genes from RNA-seq analysis of orthotopic tumors in *Il17ra*$^{-/-}$ mice compared to *Il17ra*$^{+/+}$ mice (n=4/group).

H. z-score of selected IL-17 related pathways in orthotopic tumors and ilea of *Il17ra*$^{-/-}$ mice, relative to *Il17ra*$^{+/+}$ mice from Ingenuity Pathway Analysis (IPA).

I. Relative mRNA expression measured by qPCR in orthotopic tumors (left) and ilea (right) at endpoint.

J. Representative images showing *Il17a* RNAScope staining in orthotopic tumors (left) and ileum (right). Scale bars represent 40 μm.

K.Heatmap showing foldchange (FC) of plasma cytokine levels in tumor-bearing *Il17ra*$^{-/-}$ mice compared to *Il17ra*$^{+/+}$ mice at endpoint, measured by Luminex (n=3/group).

L. Pre and post treatment plasma IL-17 levels in mice treated with either single or cocktail of antibiotics (ampicillin, vancomycin, neomycin, metronidazole and amphotericin B) in drinking water for two weeks.

M. Experimental outline of IL-17RA blockade in combination with antibiotics in PDAC subcutaneous tumor model. Starting 10 days after tumor implantation, mice were given four doses of isotype IgG or αIL-17RA monoclonal antibody with or without ampicillin treatment in drinking water until endpoint.

N. Plasma IL-17 levels at endpoint.

O. Subcutaneous tumor growth curves IL-17RA blockade in combination with ampicillin.

Data is reported as mean ± SEM; P values were calculated using Student's t test (unpaired, two tailed) for 2 groups and ANOVA for ≥2 groups; *P < 0.05, **P < 0.01, ***P < 0.001, or ****P < 0.0001.

See also Figure S1.

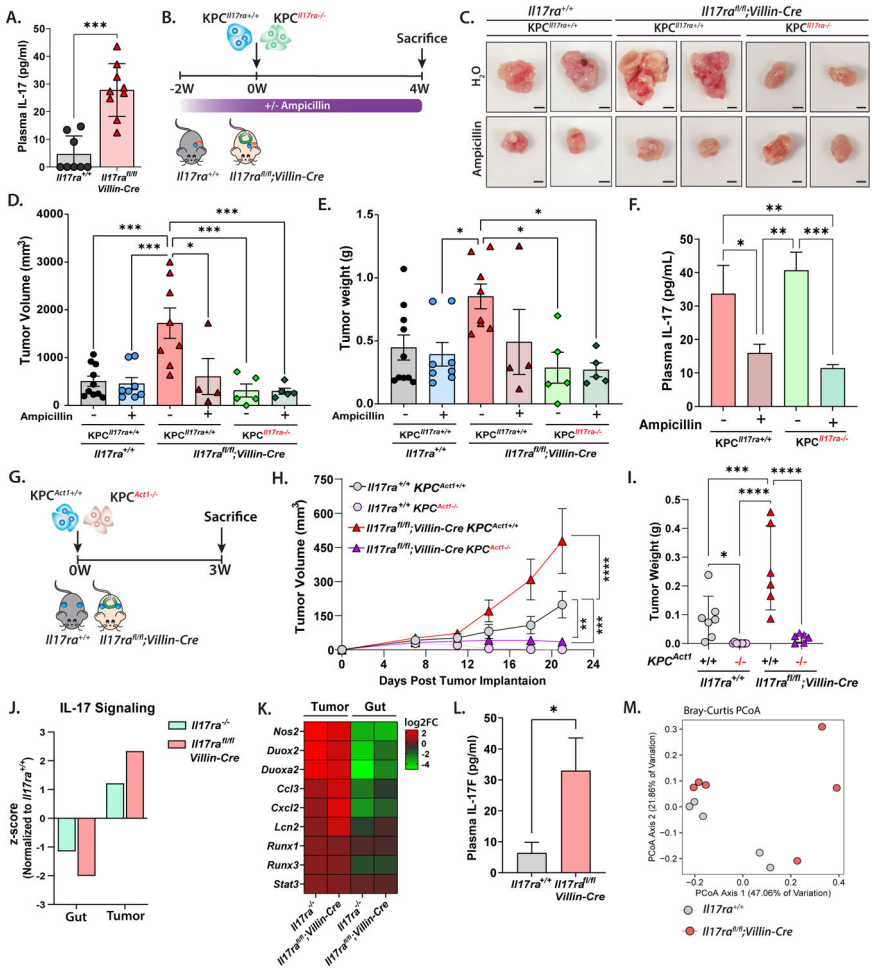

Figure 2: Enteric IL-17RA genetic deletion promotes microbially driven IL-17 signaling dependent pancreatic tumor growth.

A. Baseline plasma IL-17 levels in *Il17ra*$^{+/+}$ and *Il17ra*$^{fl/fl}$*;Villin-Cre* mice.

B. Experimental outline of murine PDAC orthotopic model. Mice were treated with ampicillin in drinking water starting from one week prior to tumor implantation. Pancreata of *Il17ra*$^{+/+}$ and *Il17ra*$^{fl/fl}$*;Villin-Cre* mice were implanted with KPC$^{Il17ra+/+}$ and KPC$^{Il17ra-/-}$ cells and sacrificed after 4 weeks.

C. Representative images (duplicates) of PDAC orthotopic tumors at endpoint. Scale bar represents 3 mm.

D-E. Orthotopic tumor volumes (D) and weight (E) at endpoint.

F. Plasma IL-17 levels in tumor-bearing *Il17ra*$^{fl/fl}$*;Villin-Cre* mice at endpoint with or without ampicillin treatment from 2B (n≥4/group).

G. Experimental outline of PDAC subcutaneous tumor model implanted with *KPC*$^{Act1+/+}$ and *KPC*$^{Act1-/-}$ cells.

H-I. Subcutaneous tumor growth curves (H) and endpoint tumor weight (I) of *KPC*$^{Act1+/+}$ and *KPC*$^{Act1-/-}$ tumors in *Il17ra*$^{+/+}$ and *Il17ra*$^{fl/fl}$*;Villin-Cre* mice.

J. z-score of the IL-17 signaling pathway in orthotopic tumors and ilea (gut) of *Il17ra*$^{-/-}$ and *Il17ra*$^{fl/fl}$*;Villin-Cre* mice, relative to *Il17ra*$^{+/+}$ mice calculated from IPA.

K. Heatmap showing log2FC of overlapping genes in tumors and ilea (gut) of *Il17ra*$^{-/-}$ and *Il17ra*$^{fl/fl}$*;Villin-Cre* mice, relative to *Il17ra*$^{+/+}$ mice from RNA-seq (n=4/group).

L. Baseline plasma IL-17F levels in tumor-bearing *Il17ra*$^{+/+}$ and *Il17ra*$^{fl/fl}$*;Villin-Cre* mice at endpoint measured by Luminex (n ≥3/group).

M. Bray-Curtis PCoA plot of beta diversity showing distance between stool samples of *Il17ra*$^{+/+}$ and *Il17ra*$^{fl/fl}$*;Villin-Cre* mice.

Data is reported as mean ± SEM; P values were calculated using Student's t test (unpaired, two tailed) for 2 groups and ANOVA for ≥2 groups; *P < 0.05, **P < 0.01, ***P < 0.001, or ****P < 0.0001.

See also Figures S2, S3 and S4.

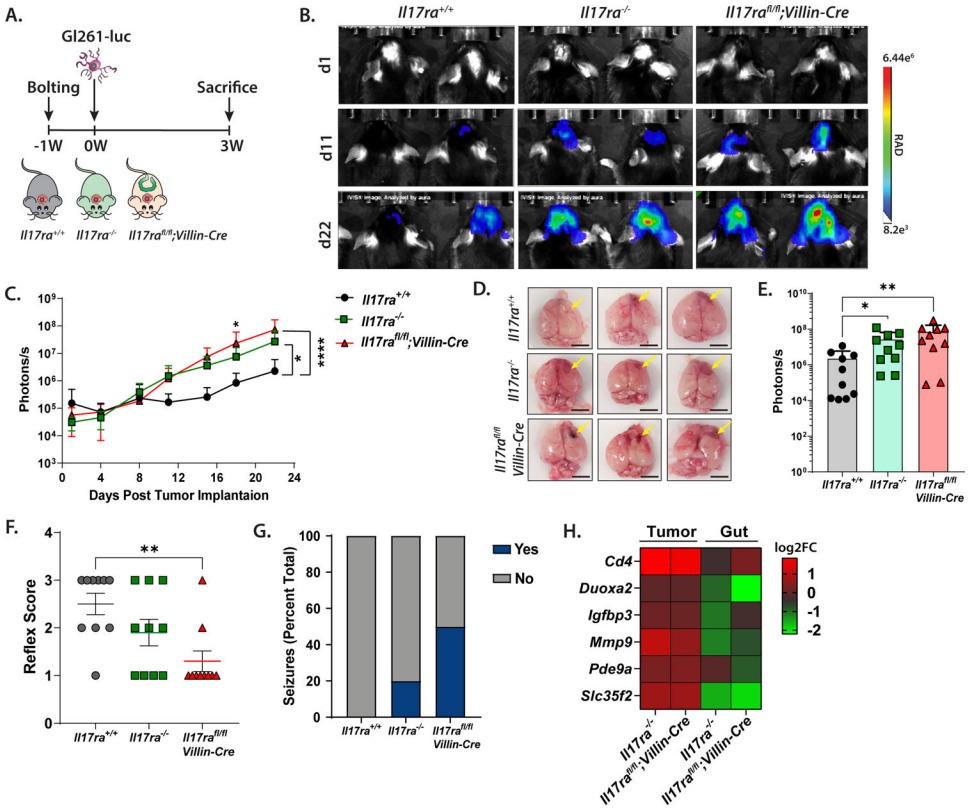

Figure 3: Intestinal IL-17-IL-17RA dependent microbial dysbiosis can affect tumor growth remotely

A. Experimental outline of murine GBM orthotopic model. Guided screws were intracranially implanted one week prior to tumor implantation. Brains of *Il17ra*$^{+/+}$, *Il17ra*$^{-/-}$ and *Il17ra*$^{fl/fl}$*;Villin-Cre* mice were implanted with murine GBM cells Gl261 and sacrificed after three weeks.

B. Representative bioluminescent images showing cranial luciferin expression in *Il17ra*$^{+/+}$, *Il17ra*$^{-/-}$ and *Il17ra*$^{fl/fl}$*;Villin-Cre* mice at day 1 (left), day 11 (middle) and day 22 (right) post implantation. Luminescence is represented as a heatmap in radians.

C. Tumor growth curves measured by bioluminescent imaging.

D. Representative images (triplicates) of GBM orthotopic tumors from *Il17ra*$^{+/+}$, *Il17ra*$^{-/-}$ and *Il17ra*$^{fl/fl}$*;Villin-Cre* mice at endpoint. Yellow arrows indicate site of tumor injection. Scale bar represents 3 mm.

E. Tumor volumes at endpoint measured by bioluminescent imaging.

F-G. Neurological symptoms- reflex score (F) and presence of seizures (G) in *Il17ra*$^{+/+}$, *Il17ra*$^{-/-}$ and *Il17ra*$^{fl/fl}$*;Villin-Cre* mice at endpoint.

H. Heatmap showing log2FC of genes in GBM orthotopic tumors and ilea of *Il17ra*$^{-/-}$ and *Il17ra*$^{fl/fl}$*;Villin-Cre* mice, relative to tumors and ilea of *Il17ra*$^{+/+}$ mice assessed from RNA-seq (n=4/group).

Data is reported as mean ± SEM; P values were calculated using Student's t test (unpaired, two tailed) for 2 groups and ANOVA for ≥2 groups; *P < 0.05, **P < 0.01, ***P < 0.001, or ****P < 0.0001.

See also Figure S4.

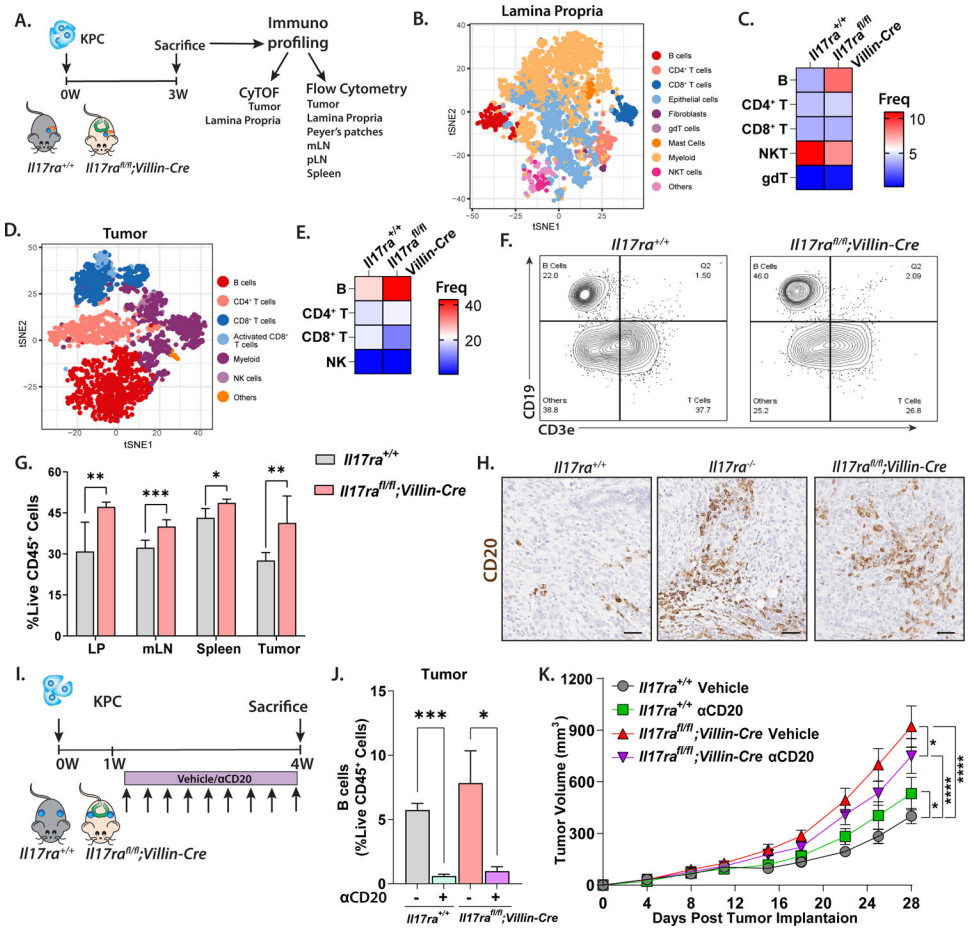

Figure 4: Enteric IL-17RA deficiency triggers B cells development

A. Experimental outline of murine PDAC orthotopic model. Pancreata of *Il17ra*$^{+/+}$ and *Il17ra*$^{fl/fl}$*;Villin-Cre* mice were implanted with KPC cells sacrificed after 3 weeks for immunoprofiling of tumor, lamina propria (LP), Peyer's patches (PP), mesenteric lymph nodes (mLN), pancreatic lymph nodes (pLN) and spleen; via CyTOF and flow cytometry.

B-C. viSNE plot (B) and lymphocytic populations (C) in LP from *Il17ra*$^{+/+}$ and *Il17ra*$^{fl/fl}$*;Villin-Cre* mice (n=3/group).

D-E. viSNE plot (D) and lymphocytic populations (E) in tumors from *Il17ra*$^{+/+}$ and *Il17ra*$^{fl/fl}$*;Villin-Cre* mice (n=3/group).

F. Representative flow cytometric plot showing immune populations in orthotopic tumors of *Il17ra*$^{+/+}$ and *Il17ra*$^{fl/fl}$*;Villin-Cre* mice.

G. Quantification of B cells abundance in LP, mLN, spleen and tumors by flow cytometric analysis, reported as a percent of viable CD45^{+} cells.

H. Representative images showing CD20 IHC staining in orthotopic KPC tumors from *Il17ra*$^{+/+}$, *Il17ra*$^{-/-}$ and *Il17ra*$^{fl/fl}$*;Villin-Cre* mice. Scale bar represents 50 μm.

I. Experimental outline of *in vivo* B cell depletion in PDAC subcutaneous tumor model using neutralizing antibodies against αCD20.

J. Levels of B cells in tumors reported as a percent of viable CD45^{+} cells, measured by flow cytometry.

K. Growth curves of subcutaneous tumors with B cell depletion in *Il17ra*$^{+/+}$ and *Il17ra*$^{fl/fl}$*;Villin-Cre* mice.

Data is reported as mean ± SEM; P values were calculated using Student's t test (unpaired, two tailed) for 2 groups and ANOVA for ≥2 groups; *P < 0.05, **P < 0.01, ***P < 0.001, or ****P < 0.0001.

See also Figure S5 and Table S1.

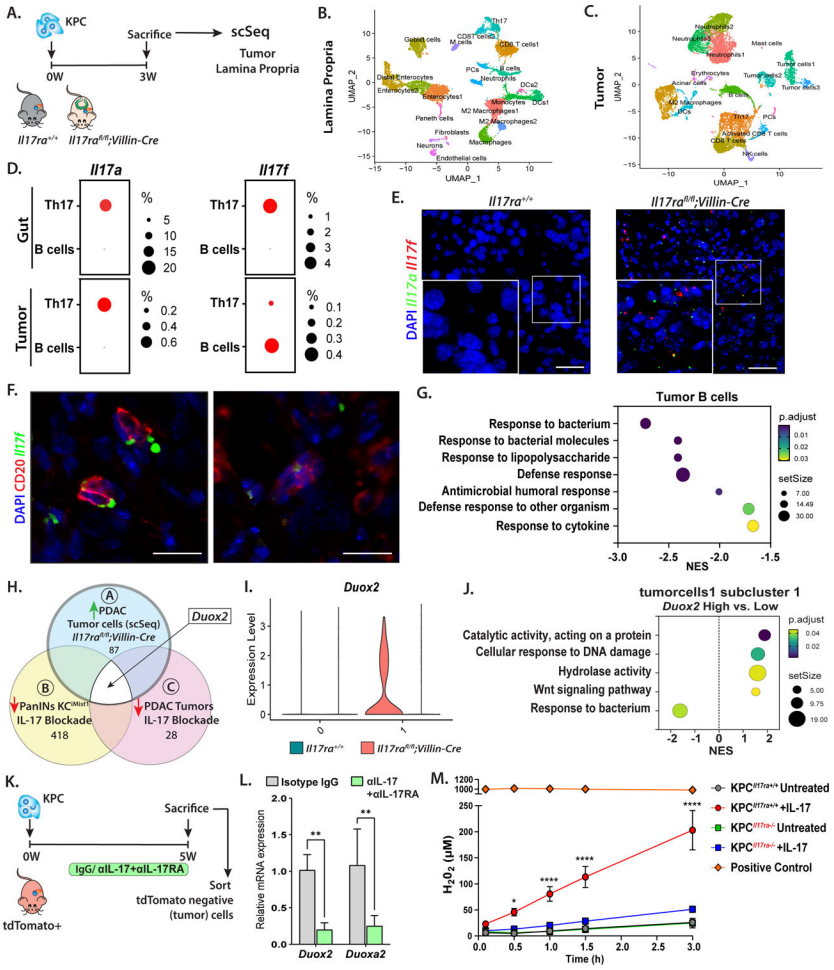

Figure 5: Enteric IL-17RA deficiency driven dysbiosis rewires immune and tumor cells

A. Experimental outline of murine PDAC orthotopic model. Pancreata of *Il17ra*$^{+/+}$ and *Il17ra*$^{fl/fl}$*;Villin-Cre* mice were implanted with KPC cells sacrificed after 3 weeks for single cell RNA sequencing (scRNA-seq) of matched tumor and lamina propria (gut) samples.

B. UMAP plot showing cell clusters in ilea (gut) samples of tumor bearing *Il17ra*$^{fl/fl}$*;Villin-Cre* and *Il17ra*$^{+/+}$ mice (n=2/group).

C. UMAP plot showing cell clusters in matched tumors samples of *Il17ra*$^{fl/fl}$*;Villin-Cre* and *Il17ra*$^{+/+}$ mice (n=3/group).

D. Dot plots showing *Il17a* (left) and *Il17f* (right) average expression in Th17 and B cells in gut (top) and tumor (bottom) samples from *Il17ra*$^{fl/fl}$*;Villin-Cre* mice assessed from single cell analysis.

E. RNAScope staining showing *Il17a* and *Il17f* expression in pancreatic orthotopic tumors from *Il17ra*$^{+/+}$ and *Il17ra*$^{fl/fl}$*;Villin-Cre* mice. Scale bar represents 40 μm.

F. RNAScope staining showing *Il17f* and CD20+ cells in pancreatic orthotopic tumors from *Il17ra*$^{fl/fl}$*;Villin-Cre* mice. Scale bar represents 20 μm.

G. Enriched pathway in tumor B cells cluster from GSEA analysis in *Il17ra*$^{fl/fl}$*;Villin-Cre* vs. *Il17ra*$^{+/+}$ mice.

H. Venn diagram showing overlapping genes in IL-17 driven pancreatic datasets (Table S2): a) upregulated genes in 'Tumor cells1' cluster from single cell analysis (scRNA-seq) from advanced pancreatic tumors of *Il17ra*$^{fl/fl}$*;Villin-Cre*, b) downregulated genes in PanINs (premalignant pancreas) of KC^{iMist1} mice receiving IL-17 blockade[27] and c) downregulated genes in advanced pancreatic tumors of WT mice receiving IL-17 blockade[30].

I. Violin plot showing *Duox2* expression in sub clusters of 'Tumor cells1' divided by *Duox2* expression in *Il17ra*$^{+/+}$ and *Il17ra*$^{fl/fl}$*;Villin-Cre* mice.

J. Enriched pathways from GSEA analysis in 'Tumor cells1' sub cluster 1 (*Duox2* High) in *Il17ra*$^{fl/fl}$*;Villin-Cre* vs *Il17ra*$^{+/+}$ mice.

K. Experimental outline of murine pancreatic orthotopic model. Pancreata of whole body tdTomato+ mice were implanted with KPC cells and treated with αIL-17+αIL-17RA twice a week starting at day 10. At sacrifice, tdTomato negative (tumor cells) were enriched by sorting.

L. Relative mRNA expression of *Duox2* and *Duoxa2* measured by qPCR in tumors.

M. Quantification of H_2O_2 released over time by KPC$^{Il17ra+/+}$ and KPC$^{Il17ra-/-}$ cells treated with IL-17 *in vitro*, measured by Amplex Red assay. Experiment was repeated at least thrice. Data is reported as mean ± SEM; P values were calculated using Student's t test (unpaired, two tailed) for 2 groups and ANOVA for ≥2 groups; *P < 0.05, **P < 0.01, or ****P < 0.0001.

See also Figures S6, S7 and Table S2.

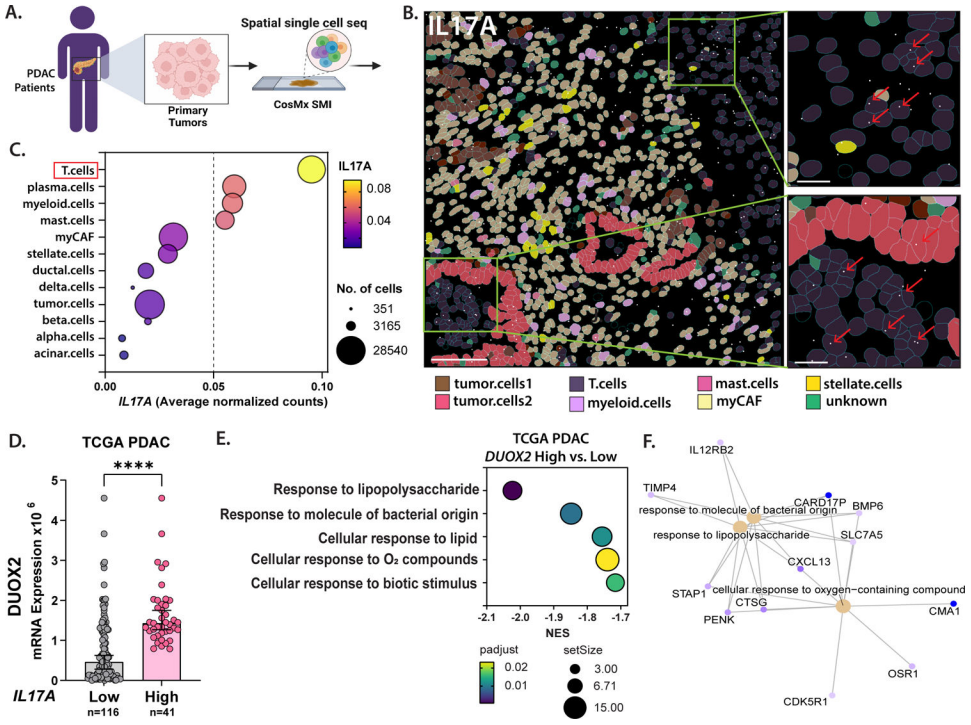

Figure 6: Human PDAC has circulating and tumor infiltrating IL-17-expressing cells that associate with DUOX2

A. Experimental outline of spatial single cell transcriptomic profiling of clinical PDAC primary tumors by CosMx Spatial Molecular Profiling (SMI).

B. Representative image showing *IL17A* transcripts (white) across cell types in selected ROIs. Scale bar represents 125 μm (left) and 25 μm (right, insets).

C. Bubble plot showing average normalized counts of *IL17A* expression in each cell type cluster from CosMx SMI analysis.

D. *DUOX2* expression in TCGA PDAC patients stratified according to average *IL17A* expression.

E-F. Pathway analysis from GSEA analysis showing enriched pathways (E) and cnetplot (F) in TCGA PDAC patients stratified according to high vs. low *DUOX2* expression.

Data is reported as mean ± SEM; P values were calculated using Student's t test (unpaired, two tailed); ****P < 0.0001.

See also Figure S7.